



OPEN ACCESS

EDITED BY

Emanuel Guariglia,
São Paulo State University, Brazil

REVIEWED BY

Wenfeng Chen,
SUNY Polytechnic Institute, United States
Yanxing Yang,
Caldwell University, United States

*CORRESPONDENCE

Chokri Chniti
✉ chokri.chniti@ipein.rnu.tn

RECEIVED 28 February 2025

ACCEPTED 16 June 2025

PUBLISHED 11 July 2025

CITATION

Alzahrani SM, Chniti C and AlMutairi DM
(2025) Exact optical soliton solutions and
interaction dynamics in fractional nonlinear
systems. *Front. Appl. Math. Stat.* 11:1584929.
doi: 10.3389/fams.2025.1584929

COPYRIGHT

© 2025 Alzahrani, Chniti and AlMutairi. This is
an open-access article distributed under the
terms of the [Creative Commons Attribution
License \(CC BY\)](#). The use, distribution or
reproduction in other forums is permitted,
provided the original author(s) and the
copyright owner(s) are credited and that the
original publication in this journal is cited, in
accordance with accepted academic practice.
No use, distribution or reproduction is
permitted which does not comply with these
terms.

Exact optical soliton solutions and interaction dynamics in fractional nonlinear systems

Saleh M. Alzahrani¹, Chokri Chniti^{2*} and
Dalal Marzouq AlMutairi³

¹Department of Mathematics, University College in Al-Qunfudhah, Umm Al-Qura University, Al-Qunfudhah, Saudi Arabia, ²Preparatory Institute for Engineering Studies of Nabeul, University of Carthage, Nabeul, Tunisia, ³Department of Mathematics, College of Science and Humanities, Shaqra University, Al-Dawadmi, Saudi Arabia

This paper aims to provide a rigorous analytical investigation of multisoliton dynamics within a conformable concatenated nonlinear framework that unifies the nonlinear Schrödinger, Sasa Satsuma, and Lakshmanan Porsezian Daniel equations through the incorporation of a conformable fractional derivative. By extending classical calculus to encompass fractional-order dynamics, the model captures intricate higher-order dispersion and non-linear interactions that critically influence pulse propagation in optical fibers. Employing advanced techniques such as the modified simplest equation method and the Kudryashov method, we derive a comprehensive family of exact soliton solutions including bright, dark, and mixed profiles and establish explicit parameter relations governing their stability and evolution. Detailed numerical simulations further elucidate the effects of the fractional parameter on soliton propagation, interaction dynamics, and energy conservation.

KEYWORDS

conformable fractional derivative, nonlinear Schrödinger equation, Sasa Satsuma equation, modified simplest equation method, Kudryashov method, optical fiber dynamics, multi-soliton interactions

1 Introduction

In recent years, there has been an unprecedented surge in the exploration of nonlinear mathematical models aimed at describing pulse propagation in optical fibers. These models play a critical role in advancing our understanding of wave dynamics [1], enabling significant progress in fields such as nonlinear optics, plasma physics, fluid dynamics, and quantum mechanics [2–4]. Among these, the nonlinear Schrödinger equation (NLSE) stands out as a fundamental model that provides a framework for studying various soliton solutions, which are essential for describing stable waveforms capable of maintaining their structure over long distances [5]. Soliton solutions hold a prominent place in scientific research due to their applications in fiber optic communication, signal processing, and data transmission [5–7]. They are indispensable for enhancing the efficiency and reliability of global communication networks cornerstones of modern technological infrastructure. By maintaining their shape and amplitude through nonlinear and dispersive effects, solitons mitigate signal degradation, thereby facilitating long-distance data transmission without distortion. The growing interest in soliton theory has driven the development of advanced analytical and numerical techniques for deriving soliton solutions to nonlinear evolution equations [8]. Researchers have explored numerous nonlinear physical models to predict soliton behavior under various conditions, fostering breakthroughs in nonlinear optics

and ferromagnetic materials [9–11]. Optical solitons, in particular, stand out for their ability to resist dispersive spreading, making them invaluable for applications in photonic circuits, high-speed data networks, and optical switching technologies. Soliton solutions are generally classified into bright, dark, and mixed forms, each exhibiting distinct physical characteristics and applications. Bright solitons are mobile, traveling through a medium with a localized peak, and are commonly employed in data transmission systems. In contrast, dark solitons manifest as localized dips in the continuous wave background, often remaining stationary or exhibiting minimal mobility. This stationary nature, termed quiescence, results from a precise balance between nonlinear effects and dispersive forces, making dark solitons ideal for stable, localized light sources. The versatility of soliton solutions extends to mixed dark-bright solitons, enabling more intricate pulse shaping for specialized optical applications [12–14]. Despite the wide-ranging applications of soliton solutions, the inherent complexity of nonlinear equations often presents challenges in obtaining explicit analytical solutions. As a result, sophisticated mathematical methods are essential for deriving accurate solutions to these intricate models. Notable approaches include the Sardar sub-equation method [15, 16], the modified extended tanh-function method [17, 18], the Riccati expansion method [19], the generalized exponential rational function method [20, 21], and the generalized Arnous method [22]. Each of these techniques contributes uniquely to the field, broadening our understanding of nonlinear wave dynamics and soliton interactions under perturbative conditions. This study delves into a concatenated model that merges three significant equations: the Sasa Satsuma (SS) equation, the Lakshmanan Porsezian Daniel (LPD) equation, and the nonlinear Schrödinger equation (NLSE) [23, 24]. The concatenation of these models provides a more comprehensive framework for examining nonlinear wave phenomena, capturing the combined effects of higher-order dispersion, self-phase modulation, and nonlinear interactions. This integrated model plays a crucial role in investigating soliton dynamics in complex optical systems and diverse waveguiding structures. The core focus of this paper is to derive and analyze novel soliton solutions within the conformable concatenation model, characterized by the presence of a conformable derivative. This approach generalizes classical derivative definitions by incorporating fractional-order dynamics, thereby enabling more accurate modeling of nonlinearity and dispersion at finer scales. Several formulations of fractional derivatives in the complex plane have been introduced to expand analytical capabilities [25]. Notably, Li et al. conducted an in-depth investigation into the properties of fractional operators in complex domains, further advancing traditional formulations [26]. For additional theoretical developments and broader mathematical perspectives on fractional calculus and its applications, we refer the reader to [27–31].

This study focuses on the conformable concatenation model, which unifies the nonlinear Schrödinger equation (NLSE), the Lakshmanan Porsezian Daniel (LPD) model, and the Sasa Satsuma (SS) equation [32]. This integrated framework allows for a comprehensive analysis of nonlinear wave dynamics by capturing the combined effects of higher-order dispersion, cubic and quintic nonlinearities, and self-phase modulation. The concatenation

model facilitates the exploration of complex soliton interactions and pulse propagation behaviors, providing deeper insights into the nonlinear optical systems governed by these equations. The soliton solutions derived in this study possess direct physical relevance in optical fiber communication and nonlinear wave dynamics. In practical terms, bright solitons modeled by the conformable framework are essential for long-distance data transmission in anomalous dispersion regimes, as they maintain their shape and amplitude over time, minimizing signal distortion in high-capacity fiber networks. Dark solitons, on the other hand, are suited for applications such as optical switching and signal gating in normal dispersion settings, offering enhanced stability and localization. Notably, these soliton types can be applied to two-mode optical fibers and soliton wavelength-division multiplexing systems, where managing multiple pulse channels requires precise control over nonlinear and dispersive dynamics [33]. The incorporation of the conformable fractional derivative introduces tunable control over dispersion and nonlinearity, reflecting the behavior of complex photonic media with memory or nonlocal effects. This fractional framework aligns with recent advances in modeling coupled nonlinear Schrödinger systems that govern pulse propagation in structured fiber channels [33]. Such flexibility is particularly advantageous for emerging technologies like adaptive waveguides, programmable photonic circuits, and 5G backbone infrastructure. Furthermore, the multi-soliton interaction dynamics, including energy exchange and peak modulation, provide insights relevant to soliton-based logic gates, wavelength-division multiplexing, and nonlinear optical filtering, reinforcing the practical utility of the solutions across a range of optical and photonic systems. The structure of the paper is the following. In Section 2, we present a brief review of solitary waves. In Section 3, we introduce the governing conformable concatenated nonlinear model, which merges the Sasa–Satsuma equation, the Lakshmanan–Porsezian–Daniel equation, and the nonlinear Schrödinger equation. In Section 4, the modified simplest equation method is applied to derive exact optical soliton solutions for the conformable concatenation model. This process includes balancing terms, solving the resulting algebraic system, and constructing explicit soliton profiles. In Section 5, we explore the application of the Kudryashov method to obtain additional soliton solutions. Soliton dynamics are further investigated, and a detailed analysis of peak intensities, spatial profiles, and propagation behaviors is provided. Multi-soliton interactions and collisions are examined, including energy conservation during soliton encounters. Finally, we conclude in Section 6.

2 Solitary waves

The concept of solitons, or solitary waves, dates back to the early 19th century, when Scottish civil engineer and naval architect John Scott Russell made the first recorded observation [34]. Russell identified what he termed the “great wave of translation” and conducted extensive water tank experiments to investigate its fundamental properties. Although he emphasized the wave’s significance, his claims were initially met with skepticism by the scientific community. Historically, George Airy and George

G. Stokes attempted to explain solitary waves theoretically, but without success. Airy incorrectly attributed them to his linear shallow water theory, while Stokes questioned their persistence. The first formal theoretical descriptions of solitary waves came from Boussinesq in 1871 and Rayleigh in 1876. However, substantial progress occurred in 1895, when Korteweg and de Vries introduced the renowned KdV equation [35]. Despite this advancement, the full significance of solitary waves was not recognized until 1965, when Zabusky and Kruskal conducted a numerical analysis of the KdV equation [36]. Their simulations revealed that solitary waves behave like particles, maintaining their shape and speed after interactions, leading them to coin the term “solitons.” Since then, solitons have found applications in various areas of applied science. In particular, many integrable dynamical systems have been shown to admit soliton solutions, which can be studied through the inverse scattering transform (IST) a nonlinear analog of the Fourier transform for linear partial differential equations. Developed by Gardner, Greene, Kruskal, and Miura, the IST is regarded as one of the most significant breakthroughs in 20th-century mathematical physics [37]. Solitons arise as solutions to specific nonlinear partial differential equations characterized by the presence of nonlinear terms within their structure [38].

3 Mathematical formulation

The model is expressed as:

$$\begin{aligned} i \left(\frac{\partial^\alpha \Phi}{\partial t^\alpha} \right) + a \frac{\partial^2 \Phi}{\partial x^2} + b |\Phi|^2 \Phi \\ + c_1 \left(\tau_1 \frac{\partial^4 \Phi}{\partial x^4} + \tau_2 \left(\frac{\partial \Phi}{\partial x} \right)^2 \Phi^* + \tau_3 \left| \frac{\partial \Phi}{\partial x} \right|^2 \Phi \right. \\ \left. + \tau_4 |\Phi|^2 \frac{\partial^2 \Phi}{\partial x^2} + \tau_5 \Phi^2 \frac{\partial^2 \Phi^*}{\partial x^2} + \tau_6 |\Phi|^4 \Phi \right) \\ + ic_2 \left[\tau_7 \frac{\partial^3 \Phi}{\partial x^3} + \tau_8 |\Phi|^2 \frac{\partial \Phi}{\partial x} + \tau_9 \Phi^2 \frac{\partial \Phi^*}{\partial x} \right] \\ = 0 \quad 0 < \alpha \leq 1. \end{aligned} \quad (1)$$

where $\Phi(x, t)$ represents the wave profile, a signifies chromatic dispersion, b denotes Kerr nonlinearity and τ_i encapsulate higher-order dispersion terms. The term $\frac{\partial^\alpha}{\partial t^\alpha}$ represents the conformable fractional derivative, a pivotal component that enhances the accuracy of soliton modeling by incorporating fractional dynamics. This definition generalizes the classical derivative to accommodate memory and nonlocal effects inherent in complex optical media. The Equation 1 models the propagation of optical pulses where the second derivative captures dispersion and the nonlinear terms model self-phase modulation and higher-order effects.

The parameter $\alpha \in (0, 1]$ in the model represents the order of the conformable fractional time derivative and governs the degree of memory and nonlocal temporal effects in the evolution of the optical field $\Phi(x, t)$. When $\alpha = 1$, the model reduces to the classical (integer-order) nonlinear Schrödinger-type equation, recovering standard dispersive and nonlinear dynamics. Values $\alpha < 1$ introduce fractional temporal behavior, which accounts for complex physical mechanisms such as anomalous dispersion, non-instantaneous nonlinear response, or temporal heterogeneity

in the propagation medium. While mathematically general, the use of fractional α also has physical relevance in optical systems where pulse propagation is influenced by viscoelasticity, nonlocal media, or memory effects.

This formulation not only extends the classical nonlinear Schrödinger framework but also allows for a more refined representation of pulse evolution in optical fibers, accounting for nonlinearity and dispersion effects at varying temporal scales.

Definition 3.1. The fractional derivative is defined as [39]:

$$L_\beta(q)(z) = \lim_{d \rightarrow 0} \frac{\Phi(z + dz^{1-\beta}) - \Phi(z)}{d}, \quad \beta \in (0, 1]. \quad (2)$$

where Φ_1 and Φ_2 are conformable differentiable of order β , and $s_1, s_2 \in \mathbb{R}$.

Properties 3.1. The following properties hold [39]:

1. $L_\beta(s_1 \Phi_1 + s_2 \Phi_2) = s_1 L_\beta(\Phi_1) + s_2 L_\beta(\Phi_2)$.
2. $L_\beta(x^l) = l x^{l-\beta}$ for all $l \in \mathbb{R}$.
3. $L_\beta(\Phi_1 \Phi_2) = \Phi_2 L_\beta(\Phi_1) + \Phi_1 L_\beta(\Phi_2)$.
4. $L_\beta \left(\frac{\Phi_1}{\Phi_2} \right) = \frac{\Phi_2 L_\beta(\Phi_1) - \Phi_1 L_\beta(\Phi_2)}{\Phi_2^2}$.

The application of the conformable derivative to optical fibers enables the modeling of complex physical phenomena, such as nonlinearity and dispersion, surpassing the constraints of traditional calculus. As an extension of the classical derivative, it introduces fractional-order dynamics into mathematical models, providing a more refined description of the behavior of optical fibers. Fractional dynamics have been shown to accurately capture realistic physical behavior while ensuring numerical stability [40]. This advancement allows for improved simulations of pulse propagation and soliton dynamics. Using the conformable derivative, researchers can systematically explore how different degrees of nonlinearity and dispersion affect the stability, shape, and velocity of soliton. This flexibility is crucial for optimizing optical fibers to meet specific technological requirements. The development enhances signal processing, facilitating high-capacity data transmission, optical switching, and light-pulse management in photonic circuits. The core objective of this study is to investigate the dynamic characteristics of optical soliton solutions within a concatenated model involving fractional time, which integrates the Sasa Satsuma equation, the Lakshmanan Porseizian Daniel equation, and the nonlinear Schrödinger equation. To achieve this, the research employs advanced methods, including the modified simplest equation technique and the Kudryashov approach, yielding novel optical solutions applicable to diverse aspects of pulse propagation in optical fibers.

To place the proposed model in perspective, we note that the classical nonlinear Schrödinger equation (NLSE) effectively describes soliton propagation under Kerr nonlinearity but does not incorporate higher-order dispersion or nonlocal effects [41]. The Sasa-Satsuma (SS) equation addresses third-order dispersion and self-steepening terms [42], while recent studies have extended the NLS framework to include fourth-order effects, enabling the derivation of more intricate soliton structures using algebraic techniques [5]. However, these models do not capture fractional temporal dynamics. By introducing a conformable fractional

derivative, our concatenated model offers enhanced flexibility for modeling complex dispersive and nonlinear phenomena in optical media, albeit with increased analytical complexity.

Equation 1 governs the evolution of a complex wave function $\Phi(x, t)$, which typically represents the envelope of an optical field and may carry internal degrees of freedom such as polarization or charge. In principle, such equations are expected to originate from a variational principle via the Euler-Lagrange formalism, ensuring the conservation of associated physical quantities. However, the presence of explicit conjugate terms such as $\left(\frac{\partial \Phi}{\partial x}\right)^2 \Phi^*$ and $\Phi^2 \frac{\partial^2 \Phi^*}{\partial x^2}$ indicates that Equation 1 does not arise from a conventional Lagrangian and may violate conservation laws such as charge conservation. This suggests that the model is phenomenological in nature, constructed to capture essential nonlinear and higher-order dispersive effects, such as self-steepening and non-Kerr nonlinearities rather than to enforce strict symmetry constraints. Its utility lies in modeling pulse dynamics in complex optical media, where such non-conservative effects are physically relevant.

We employ the following wave transformation:

$$\Phi(x, t) = \Psi(\xi) e^{i\theta(x, t)}, \quad (3)$$

where $\Psi(\xi)$ represents the amplitude component of the wave, and $\theta(x, t)$ is the phase function. The variable ξ is defined as the traveling wave coordinate:

$$\xi = h \left(x - \frac{vt^\alpha}{\alpha} \right), \quad (4)$$

where v is the soliton velocity. The phase function $\theta(x, t)$ takes the form:

$$\theta(x, t) = -kx + \frac{wt^\alpha}{\alpha} + \phi, \quad (5)$$

where k is the wave number, ω is the angular frequency, and ϕ is the phase offset. These transformations convert the PDE into an ODE, simplifying the analysis and focusing on the traveling wave profile.

By substituting the wave transformation into the original governing equation, the problem is reduced to an ordinary differential equation in terms of $\Psi(\xi)$. This transformation simplifies the analysis and facilitates the derivation of soliton solutions. The constant ϕ represents the phase center, w denotes the soliton wave, k stands for the soliton frequency, and v represents the soliton velocity. By inserting the wave transformation (Equation 3) into the governing Equation 1, the equation separates into its real and imaginary components. The real part yields a fourth-order nonlinear ordinary differential equation.

$$\begin{aligned} c_1 \tau_1 h^4 \Psi^{(4)}(\xi) + (c_1 \tau_4 h^2 + c_1 \tau_5 k^2) \Psi(\xi)^2 \Psi''(\xi) + (c_1 \tau_1 h^2 \\ + c_1 \tau_3 h^2) \Psi(\xi) \Psi''(\xi)^2 + (ah^2 - 6c_1 \tau_1 h^2 k^2 \\ + 3c_2 \tau_7 k^2) \Psi''(\xi) + c_1 \tau_6 \Psi(\xi)^5 \\ + (b - c_1 \tau_2 k^2 + c_1 \tau_3 k^2 - c_1 \tau_4 k^2 - c_1 \tau_5 k^2 \\ + c_2 \tau_8 k - c_2 \tau_9 k) \Psi(\xi)^3 + (c_1 \tau_1 k^4 - c_2 \tau_7 k^3 \\ - ak^2 - w) \Psi(\xi) = 0, \end{aligned} \quad (6)$$

This fourth-order ODE governs the soliton structure by capturing the intricate balance between higher-order dispersion and nonlinear effects. The imaginary part, in contrast, leads to a lower-order equation involving first and third derivatives:

$$\begin{aligned} (c_2 \tau_7 h^3 - 4c_1 \tau_1 h^3 k) \Psi^{(3)}(\xi) + (4c_1 \tau_1 h k^3 - 3c_2 \tau_7 h k^2 - 2ahk \\ - hw) \Psi'(\xi) + (2c_1 \tau_5 h k - 2c_1 \tau_2 h k - 2c_1 \tau_4 h k \\ + c_2 \tau_8 h + c_2 \tau_9 h) \Psi(\xi)^2 \Psi'(\xi) = 0. \end{aligned} \quad (7)$$

This lower-order equation imposes constraints on the phase and velocity of the traveling wave, enabling consistent separation of amplitude and phase dynamics.

Starting with Equation 7, we can isolate and express the variables v and k explicitly. More precisely, v and k are given by:

$$\begin{aligned} v = 4c_1 \tau_1 k^3 - 3c_2 \tau_7 k^2 - 2ak, \quad k = \frac{c_2 \tau_7}{4c_1 \tau_1}, \\ \tau_2 = \frac{2\tau_1(\tau_8 + \tau_9)}{\tau_7} - \tau_4 + \tau_5. \end{aligned} \quad (8)$$

Equation 6 can be rewritten as:

$$\begin{aligned} \varrho_1 \Psi^{(4)}(\xi) + \varrho_2 \Psi(\xi)^2 \Psi''(\xi) + \varrho_3 \Psi(\xi) \Psi'(\xi)^2 + \varrho_4 \Psi''(\xi) \\ + \varrho_5 \Psi(\xi)^5 + \varrho_6 \Psi(\xi)^3 + \varrho_7 \Psi(\xi) = 0, \end{aligned} \quad (9)$$

where

$$\begin{aligned} \varrho_1 = c_1 \tau_1 h^4, \quad \varrho_5 = c_1 \tau_6, \\ \varrho_2 = c_1 (\tau_4 + \tau_5) h^2, \quad \varrho_6 = b + k^2 (-c_1 \tau_2 + c_1 \tau_3 \\ - c_1 \tau_4 - c_1 \tau_5) + k(c_2 \tau_8 - c_2 \tau_9), \\ \varrho_3 = c_1 (\tau_1 + \tau_3) h^2, \quad \varrho_7 = c_1 \tau_1 k^4 - c_2 \tau_7 k^3 - ak^2 - w, \\ \varrho_4 = ah^2 - 6c_1 \tau_1 h^2 k^2 \\ + 3c_2 \tau_7 h^2 k. \end{aligned} \quad (10)$$

4 Derivation of optical soliton solutions using the modified simplest equation method

We derive new conformable optical soliton solutions for the conformable concatenation model by applying the modified simplest equation method. This powerful analytical technique is instrumental in solving nonlinear differential equations that arise in optical fiber models and wave propagation studies. The method facilitates the construction of closed-form solutions, which are crucial for understanding the dynamics of solitons and their stability in nonlinear systems.

We begin by assuming that the solution to Equation 9 follows the form of a finite series expansion:

$$\Psi(\xi) = \eta_0 + \sum_{i=1}^N \eta_i \chi(\xi)^i, \quad (11)$$

where $\eta_0, \eta_1, \dots, \eta_N$ are real constants and N denotes the balancing parameter that dictates the highest power of $\chi(\xi)$ present in the expansion. This approach provides a versatile framework for approximating the complex non-linear behavior of soliton waves.

To determine the appropriate value of N , we apply the balancing principle to the highest-order derivative $\Psi^{(4)}(\xi)$ and the nonlinear term $\Psi(\xi)^5$ in Equation 9. This yields $N = 1$, simplifying the series to the following form:

$$\Psi(\xi) = \eta_0 + \eta_1 \chi(\xi), \quad (12)$$

where $\chi(\xi)$ satisfies the following nonlinear ordinary differential equation:

$$\chi'(\xi) = \gamma_0 + \chi(\xi)^2. \quad (13)$$

This relation plays a fundamental role in characterizing soliton profiles and their propagation properties. The explicit solutions to Equation 13 are obtained by analyzing the value of the parameter γ_0 . These solutions demonstrate distinct soliton behaviors in nonlinear optical systems.

Case 1: When $\gamma_0 < 0$, the solution is expressed as:

$$\begin{aligned} \chi_1(\xi) &= \sqrt{-\gamma_0} \tanh(\sqrt{-\gamma_0}(\xi + s)), \\ \chi_2(\xi) &= \sqrt{-\gamma_0} \coth(\sqrt{-\gamma_0}(\xi + s)), \\ \chi_3(\xi) &= \sqrt{-\gamma_0} \left(-\tanh(2\sqrt{-\gamma_0}(\xi + s)) \right. \\ &\quad \left. + i \operatorname{sech}(2\sqrt{-\gamma_0}(\xi + s)) \right), \\ \chi_4(\xi) &= \sqrt{-\gamma_0} \left(-\coth(2\sqrt{-\gamma_0}(\xi + s)) \right. \\ &\quad \left. + \operatorname{csch}(2\sqrt{-\gamma_0}(\xi + s)) \right), \\ \chi_5(\xi) &= \frac{\sqrt{-\gamma_0}}{2} \left(\tanh\left(\frac{\sqrt{-\gamma_0}}{2}(\xi + s)\right) \right. \\ &\quad \left. + \coth\left(\frac{\sqrt{-\gamma_0}}{2}(\xi + s)\right) \right). \end{aligned} \quad (14)$$

Case 2: If $\gamma_0 > 0$.

$$\begin{aligned} \chi_6(\xi) &= \sqrt{\gamma_0} \tan(\sqrt{\gamma_0}(\xi + s)), \\ \chi_7(\xi) &= \sqrt{\gamma_0} \cot(\sqrt{\gamma_0}(\xi + s)), \\ \chi_8(\xi) &= \sqrt{\gamma_0} \left(-\tan(2\sqrt{\gamma_0}(\xi + s)) + \sec(2\sqrt{\gamma_0}(\xi + s)) \right), \\ \chi_9(\xi) &= \sqrt{\gamma_0} \left(-\cot(2\sqrt{\gamma_0}(\xi + s)) + \csc(2\sqrt{\gamma_0}(\xi + s)) \right), \\ \chi_{10}(\xi) &= \frac{\sqrt{\gamma_0}}{2} \left(\tan\left(\frac{\sqrt{\gamma_0}}{2}(\xi + s)\right) + \cot\left(\frac{\sqrt{\gamma_0}}{2}(\xi + s)\right) \right). \end{aligned} \quad (15)$$

where s is an arbitrary integration constant. This form represents a hyperbolic tangent solution, often associated with dark solitons that maintain localized waveforms while propagating over long distances in optical fibers. By substituting Equations 12 and 13 into Equation 9, we obtain a polynomial expression involving powers of $\chi(\xi)$. The subsequent step involves systematically arranging the terms based on their respective powers and equating the coefficients of each term to zero. The following

system of algebraic equations is obtained by equating the powers of $\chi(\xi)$:

$$\begin{aligned} (\chi(\xi))^0: & \quad \varrho_5 \beta_1^5 + 2\varrho_2 \beta_1^3 + \varrho_3 \beta_1^3 + 24\varrho_1 \beta_1 = 0, \\ (\chi(\xi))^1: & \quad 5\varrho_5 \beta_0 \beta_1^4 + 4\varrho_2 \beta_0 \beta_1^2 + \varrho_3 \beta_0 \beta_1^2 = 0, \\ (\chi(\xi))^2: & \quad 10\varrho_5 \beta_0^2 \beta_1^3 + 2\varrho_2 \beta_1^3 \gamma_0 + 2\varrho_3 \beta_1^3 \gamma_0 + 2\varrho_2 \beta_0^2 \beta_1 \\ & \quad + \varrho_6 \beta_1^3 + 40\varrho_1 \beta_1 \gamma_0 + 2\varrho_4 \beta_1 = 0, \\ (\chi(\xi))^3: & \quad 10\varrho_5 \beta_0^3 \beta_1^2 + 4\varrho_2 \beta_0 \beta_1^2 \gamma_0 + 2\varrho_3 \beta_0 \beta_1^2 \gamma_0 + 3\varrho_6 \beta_0 \beta_1^2 = 0 \\ (\chi(\xi))^4: & \quad \varrho_3 \beta_1^3 \gamma_0^2 + 5\varrho_5 \beta_0^4 \beta_1 + 2\varrho_2 \beta_0^2 \beta_1 \gamma_0 + 16\varrho_1 \beta_1 \gamma_0^2 \\ & \quad + 3\varrho_6 \beta_0^2 \beta_1 + 2\varrho_4 \beta_1 \gamma_0 + \varrho_7 \beta_1 = 0, \\ (\chi(\xi))^5: & \quad \varrho_3 \beta_1^2 \beta_0 \gamma_0^2 + \varrho_5 \beta_0^5 + \varrho_6 \beta_0^3 + \varrho_7 \beta_0 = 0. \end{aligned} \quad (16)$$

Solving this system yields constraints on the solution parameters, enabling closed-form expressions for soliton profiles.

4.1 Solution of the system: first case

Upon solving the above system, we obtain the following results:

$$\begin{aligned} \varrho_1 &= \frac{-4\left(\varrho_2 + \frac{\varrho_3}{2}\right)\varrho_4\gamma_0^2 + (-2\varrho_2\varrho_7 - 2\varrho_3\varrho_7 - 2\varrho_4\varrho_6)\gamma_0 - \varrho_6\varrho_7}{32\gamma_0^2\left(\left(\varrho_2 - \frac{\varrho_3}{4}\right)\gamma_0 + \frac{\varrho_6}{2}\right)}, \\ \varrho_5 &= \frac{-16\left(\left(\varrho_2 - \frac{\varrho_3}{4}\right)\varrho_7 - \frac{3\varrho_4\varrho_2}{4}\gamma_0 - \frac{3\varrho_6\varrho_7}{4}\right)\left(\left(\varrho_2 - \frac{\varrho_3}{4}\right)\gamma_0 + \frac{\varrho_6}{2}\right)}{(6\varrho_4\gamma_0 + 5\varrho_7)^2}, \\ \beta_0 &= 0, \quad \beta_1 = -\frac{\sqrt{\gamma_0}(4\varrho_2\gamma_0 - \varrho_3\gamma_0 + 2\varrho_6)(6\varrho_4\gamma_0 + 5\varrho_7)}{\gamma_0(4\varrho_2\gamma_0 - \varrho_3\gamma_0 + 2\varrho_6)}. \end{aligned} \quad (17)$$

By incorporating Equations 3, 8, 14, and 17, we derive the following optical soliton solutions:

$$\begin{aligned} \Phi_1(x, t) &= \beta_1 \sqrt{-\gamma_0} \tanh\left(\sqrt{-\gamma_0}\left(h\left(x - \frac{\lambda_1 t^\alpha}{\alpha}\right) + s\right)\right) \\ &\quad e^{i(-kx + \frac{w t^\alpha}{\alpha} + \phi)}, \\ \Phi_2(x, t) &= \beta_1 \sqrt{-\gamma_0} \coth\left(\sqrt{-\gamma_0}\left(h\left(x - \frac{\lambda_1 t^\alpha}{\alpha}\right) + s\right)\right) \\ &\quad e^{i(-kx + \frac{w t^\alpha}{\alpha} + \phi)}, \\ \Phi_3(x, t) &= \beta_1 \sqrt{-\gamma_0} \left(-\tanh\left(2\sqrt{-\gamma_0}\left(h\left(x - \frac{\lambda_1 t^\alpha}{\alpha}\right) + s\right)\right) \right. \\ &\quad \left. + i \operatorname{sech}\left(2\sqrt{-\gamma_0}\left(h\left(x - \frac{\lambda_1 t^\alpha}{\alpha}\right) + s\right)\right) \right) e^{i(-kx + \frac{w t^\alpha}{\alpha} + \phi)}, \\ \Phi_4(x, t) &= \beta_1 \sqrt{-\gamma_0} \left(-\coth\left(2\sqrt{-\gamma_0}\left(h\left(x - \frac{\lambda_1 t^\alpha}{\alpha}\right) + s\right)\right) \right. \\ &\quad \left. + \operatorname{csch}\left(2\sqrt{-\gamma_0}\left(h\left(x - \frac{\lambda_1 t^\alpha}{\alpha}\right) + s\right)\right) \right) e^{i(-kx + \frac{w t^\alpha}{\alpha} + \phi)}, \\ \Phi_5(x, t) &= \beta_1 \sqrt{-\gamma_0} \left(\tanh\left(\frac{\sqrt{-\gamma_0}}{2}\left(h\left(x - \frac{\lambda_1 t^\alpha}{\alpha}\right) + s\right)\right) \right. \\ &\quad \left. + \coth\left(\frac{\sqrt{-\gamma_0}}{2}\left(h\left(x - \frac{\lambda_1 t^\alpha}{\alpha}\right) + s\right)\right) \right) e^{i(-kx + \frac{w t^\alpha}{\alpha} + \phi)}, \end{aligned}$$

By applying Equations 3, 8, 14, and 15, the resulting optical solutions are derived as follows:

$$\begin{aligned}\Phi_6(x, t) &= \beta_1 \sqrt{\gamma_0} \tan \left(\sqrt{\gamma_0} \left(h \left(x - \frac{\lambda_1 t^\alpha}{\alpha} \right) + s \right) \right) e^{i(-kx + \frac{wt^\alpha}{\alpha} + \phi)}, \\ \Phi_7(x, t) &= \beta_1 \sqrt{\gamma_0} \cot \left(\sqrt{\gamma_0} \left(h \left(x - \frac{\lambda_1 t^\alpha}{\alpha} \right) + s \right) \right) e^{i(-kx + \frac{wt^\alpha}{\alpha} + \phi)}, \\ \Phi_8(x, t) &= \beta_1 \sqrt{\gamma_0} \left(-\tan \left(2\sqrt{\gamma_0} \left(h \left(x - \frac{\lambda_1 t^\alpha}{\alpha} \right) + s \right) \right) + \sec \left(2\sqrt{\gamma_0} \left(h \left(x - \frac{\lambda_1 t^\alpha}{\alpha} \right) + s \right) \right) \right) e^{i(-kx + \frac{wt^\alpha}{\alpha} + \phi)}, \\ \Phi_9(x, t) &= \beta_1 \sqrt{\gamma_0} \left(-\cot \left(2\sqrt{\gamma_0} \left(h \left(x - \frac{\lambda_1 t^\alpha}{\alpha} \right) + s \right) \right) + \csc \left(2\sqrt{\gamma_0} \left(h \left(x - \frac{\lambda_1 t^\alpha}{\alpha} \right) + s \right) \right) \right) e^{i(-kx + \frac{wt^\alpha}{\alpha} + \phi)}, \\ \Phi_{10}(x, t) &= \beta_1 \sqrt{\gamma_0} \left(\tan \left(\frac{\sqrt{\gamma_0}}{2} \left(h \left(x - \frac{\lambda_1 t^\alpha}{\alpha} \right) + s \right) \right) + \cot \left(\frac{\sqrt{\gamma_0}}{2} \left(h \left(x - \frac{\lambda_1 t^\alpha}{\alpha} \right) + s \right) \right) \right) e^{i(-kx + \frac{wt^\alpha}{\alpha} + \phi)},\end{aligned}$$

where

$$\lambda_1 = -\frac{\tau_7^3 c_2^3}{8\tau_1^2 c_1^2} - \frac{a\tau_7 c_2}{2\tau_1 c_1}.$$

The curves presented in the figures are plotted using the following parameter values:

$$\begin{aligned}a &= 0.2 \quad \tau_1 = 0.1 \quad h = 0.1 \quad b = 0.2 \quad \tau_3 = 0.1 \quad c_1 = 0.1 \\ w &= 2 \quad \tau_4 = 0.5 \\ c_2 &= 0.1 \quad \tau_5 = 0.5 \quad \tau_7 = 0.7 \quad \gamma_0 = -10 \quad \tau_8 = 1 \quad \tau_9 = 2 \\ \phi &= 0.1 \quad s = 0.5\end{aligned}$$

Figure 1 presents three-dimensional (3D) intensity plots of the soliton solutions $|\Phi_1(x, t)|^2$ and $|\Phi_2(x, t)|^2$ for different values of α . The top row displays $|\Phi_1|^2$ with a hyperbolic tangent (tanh) profile, while the bottom row shows $|\Phi_2|^2$ characterized by a hyperbolic cotangent (coth) profile. The propagation of the solitons is evident along the time axis, and the plots illustrate the evolution of intensity as the solitons propagate through space. A clear decay in intensity is observed over time, highlighting the dispersive behavior of the wave. Contour plots in Figure 2 demonstrate the spatial and temporal evolution of soliton intensity for different α values. The left panels show the evolution of $|\Phi_1(x, t)|^2$, where solitons maintain a localized structure while propagating along the x-axis. On the right, $|\Phi_2(x, t)|^2$ exhibits sharper, more concentrated peaks, indicating a stronger localization effect. The contour patterns highlight how higher α values lead to faster-moving solitons with less dispersion, reinforcing the α -dependent soliton behavior. In Figure 3, the spatial profiles of $|\Phi_1|^2$ and $|\Phi_2|^2$ at a fixed time slice $t_0 = 100$ are plotted. This figure illustrates the variation in soliton

shapes as α varies. For Φ_1 , the soliton's amplitude broadens as α increases, while for Φ_2 , the soliton retains a narrow and steep profile. This contrast underscores the influence of α on soliton localization, with Φ_2 retaining a pronounced peak even at later stages. Heatmaps in Figure 4 visualize the evolution of soliton intensity over time and space for $|\Phi_1|^2$ and $|\Phi_2|^2$. The plots highlight regions of high intensity, with Φ_1 demonstrating a more gradual decay in intensity along the spatial axis. Conversely, Φ_2 exhibits sharp intensity peaks that persist over time. This figure emphasizes the differences in stability and dispersion characteristics of the two soliton types, driven by their unique mathematical profiles. Figure 5 illustrates the vector field representation of the soliton intensity gradients. This vector field reveals the flow direction of soliton energy in space and time. For lower α values, the vectors indicate slower-moving solitons with more dispersive spreading, whereas higher α values yield solitons that travel with minimal dispersion, maintaining a compact structure. The peak magnitude evolution of $|\Phi_1|^2$ and $|\Phi_2|^2$ over time is shown in Figure 6. The plot reveals that for $|\Phi_1|^2$, the peak decays smoothly, suggesting gradual energy loss. In contrast, $|\Phi_2|^2$ exhibits distinct spikes, indicating sudden intensity bursts at specific time intervals. This behavior reflects the intermittent and highly localized nature of the Φ_2 soliton compared to the more stable Φ_1 . Figure 7 depicts a waterfall plot, further illustrating the evolution of peak magnitudes for Φ_1 and Φ_2 . The soliton dynamics unfold as a function of both time and space, with Φ_1 spreading more uniformly over time. The Φ_2 soliton, maintains its peak intensity over specific regions, highlighting its robustness and reduced dispersion under certain conditions. In Figure 8, the wave front position is plotted as a function of time for different α values. The plot shows that for smaller α , the wave front moves more slowly for smaller α , and faster for larger α values. This behavior reflects the key property of fractional solitons: α modulates wave speed and affects dispersion.

The real part of the soliton wave function is visualized in Figure 9. The oscillatory nature of the Φ_1 wave is apparent, while Φ_2 exhibits significantly more localized peaks. This figure highlights the contrast between the oscillatory pattern of Φ_1 and the sharply localized nature of Φ_2 , underscoring the distinct phase behavior governed by the hyperbolic functions. Figure 10 presents soliton profiles at a fixed time, allowing for direct comparison between different α values. As α increases, the solitons become more localized and sharper. This time-slice comparison highlights the impact of α on soliton shape and spatial extent. Figure 11 presents cross-sectional views of soliton intensity profiles for various α values.

The pronounced localization and peak amplitude of Φ_2 indicate reduced dispersion relative to Φ_1 . This comparison highlights the differential spreading characteristics driven by soliton type and α variations. Additionally, Figure 12 illustrates the full temporal evolution of the soliton waves.

The gradual propagation of Φ_1 is contrasted with the sharp, distinct peaks of Φ_2 , further reflecting their unique soliton structures and temporal dynamics.

The soliton solutions Φ_1 through Φ_{10} are classified based on the sign of the Riccati parameter γ_0 , which determines the functional form of the solutions to the auxiliary equation

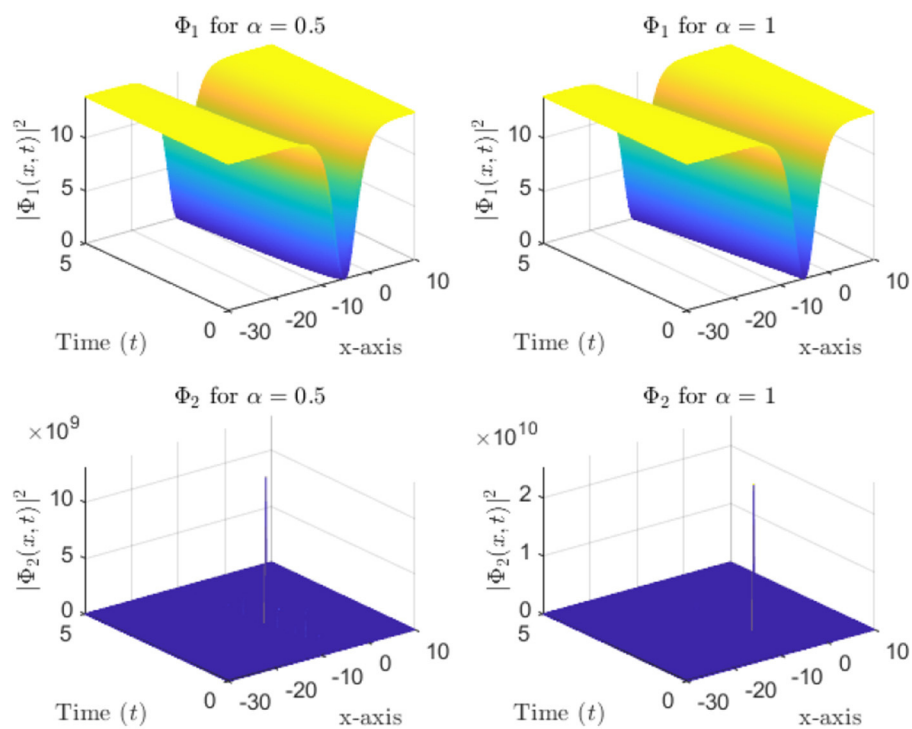


FIGURE 1
3D soliton intensity plots of $|\Phi_1(x, t)|^2$ (tanh profile) and $|\Phi_2(x, t)|^2$ (coth profile) for Various α values. (Top row), $|\Phi_1(x, t)|^2$, (Bottom row), $|\Phi_2(x, t)|^2$.

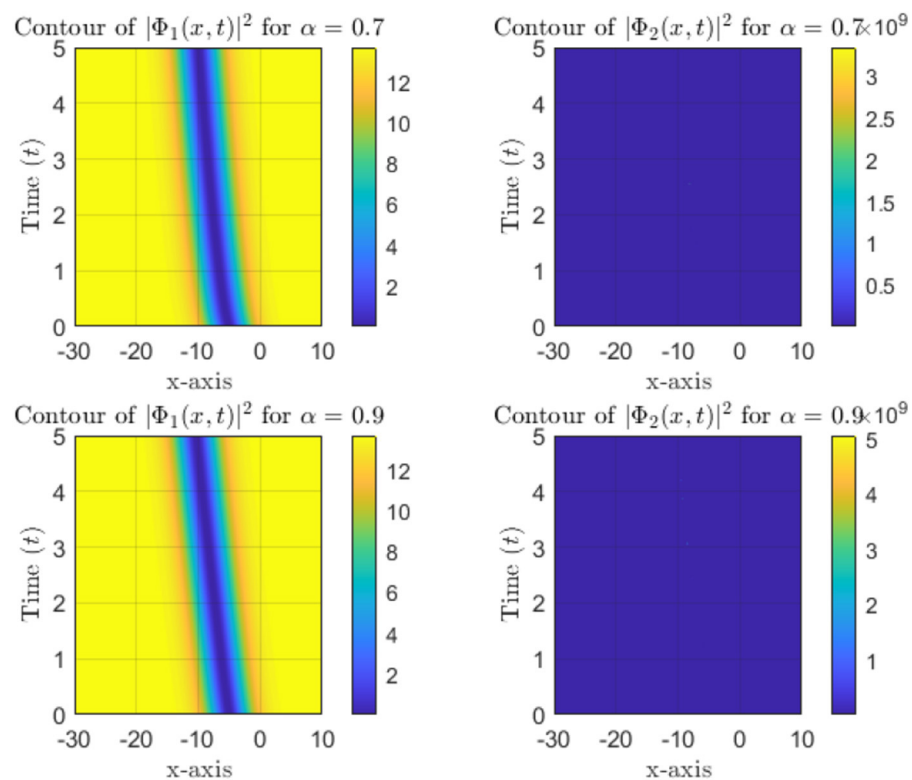


FIGURE 2
Contour plots of soliton intensity $|\Phi_1|^2$ and $|\Phi_2|^2$ for different α values, showing spatial and temporal evolution.

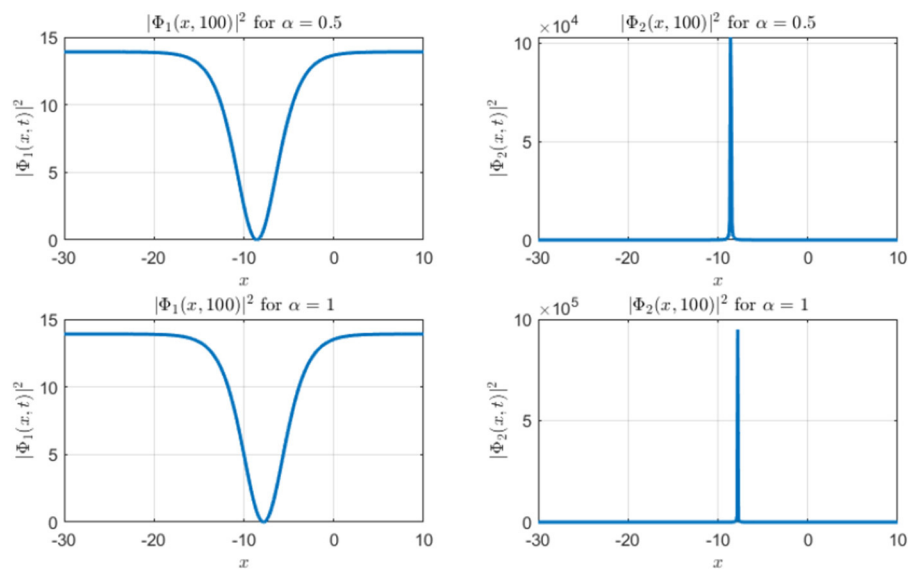


FIGURE 3
Spatial profiles of soliton intensity $|\Phi_1|^2$ and $|\Phi_2|^2$ at fixed time $t_0 = 100$.

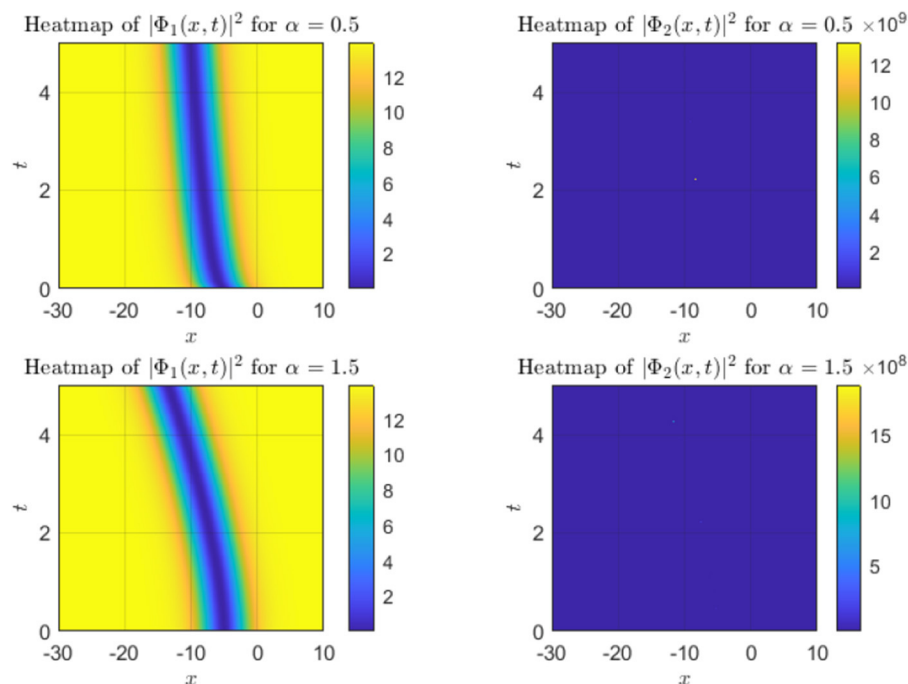


FIGURE 4
Heatmap visualization of $|\Phi_1|^2$ and $|\Phi_2|^2$ for various α values, highlighting intensity distribution over time and space.

$\chi'(\xi) = \chi^2 + \gamma_0$. Specifically, when $\gamma_0 < 0$, the solutions involve hyperbolic functions (e.g. \tanh , \coth), and when $\gamma_0 > 0$, they involve trigonometric functions (e.g. \tan , \cot). The subsequent set of solutions Φ_{11} to Φ_{20} is obtained by solving an alternative branch of the algebraic system arising from the

modified simplest equation method. Although this second case introduces different values for the algebraic parameters ρ_i , β_0 , and β_1 , classification into trigonometric or hyperbolic types remains strictly governed by the sign of γ_0 . Hence, Φ_{11} - Φ_{15} correspond to $\gamma_0 < 0$, and Φ_{16} - Φ_{20} correspond to $\gamma_0 > 0$.

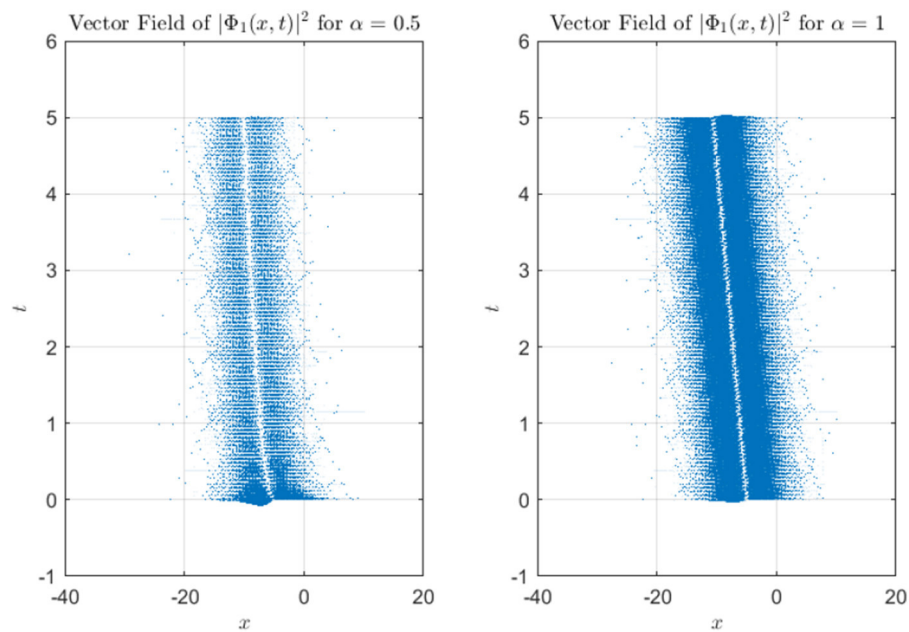


FIGURE 5

Vector field representation of soliton intensity $|\Phi_1|^2$ for different α values, depicting gradient flow in space-time.

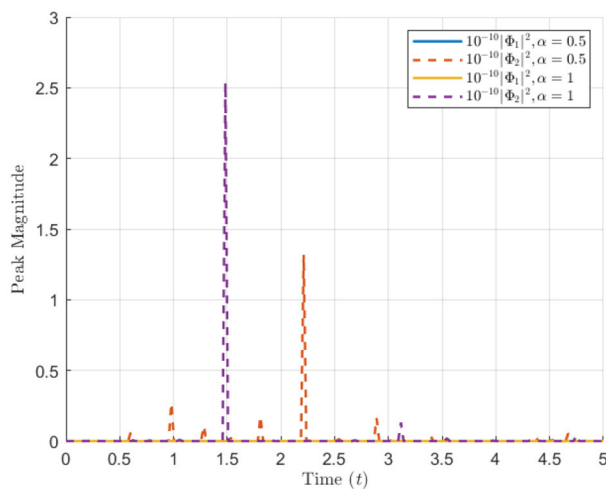


FIGURE 6

Peak magnitude evolution of $|\Phi_1|^2$ and $|\Phi_2|^2$ over time for various α values.

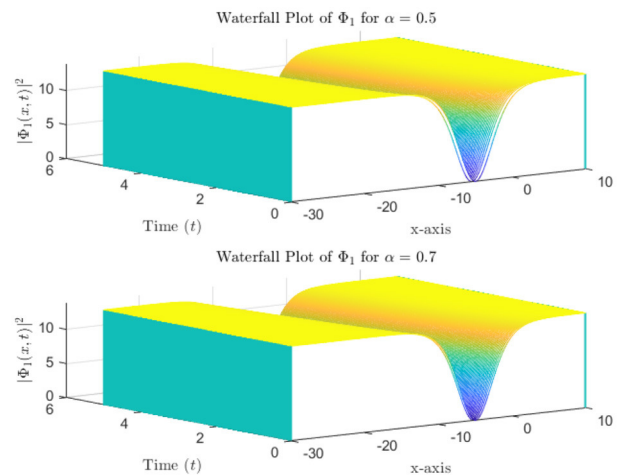


FIGURE 7

Waterfall plot showing temporal evolution of peak magnitude $|\Phi_1|^2$ and $|\Phi_2|^2$ over time.

This clarification is provided to avoid confusion: the division into cases is determined by the structure of the differential equation (through γ_0), not by the values of the algebraic coefficients themselves.

4.2 Solution of the system: second case

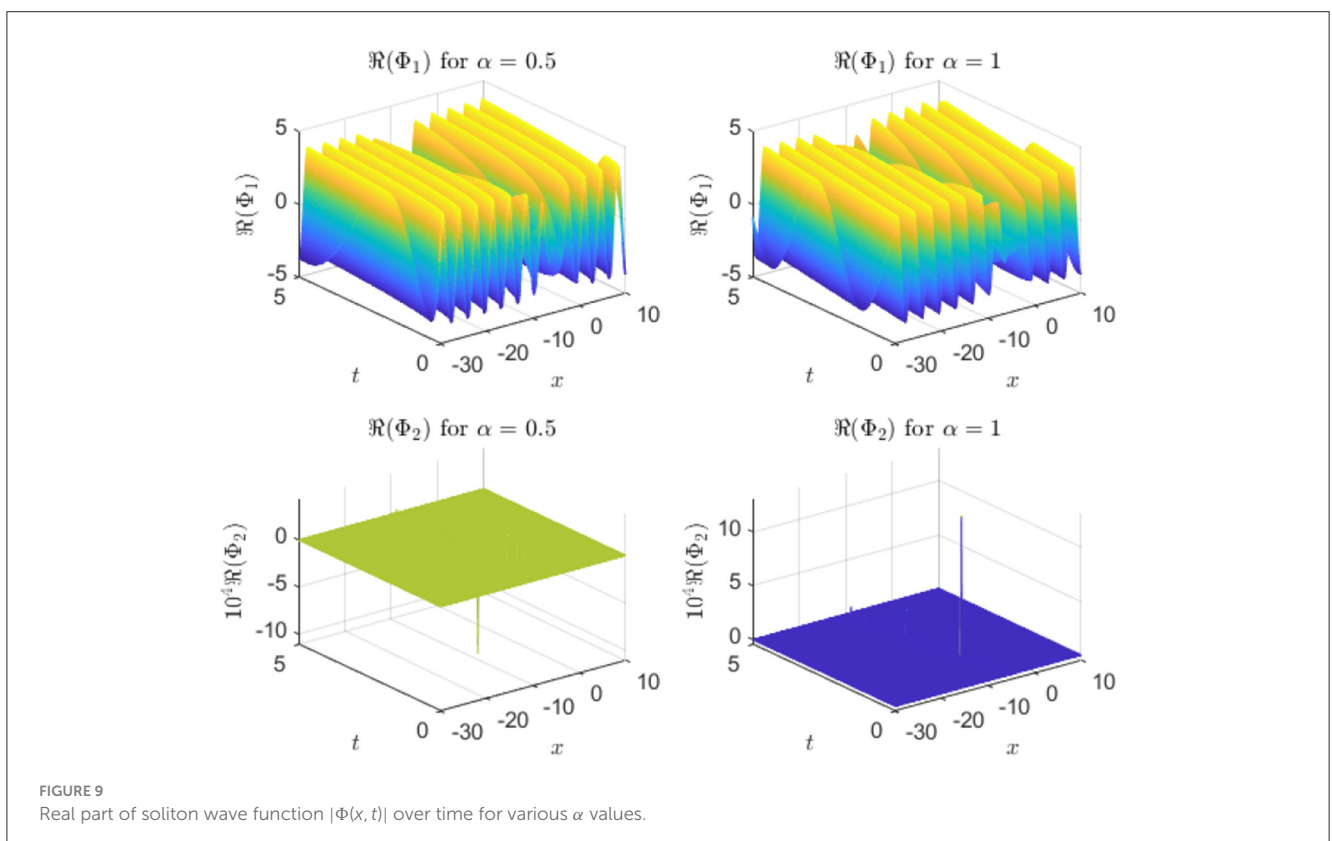
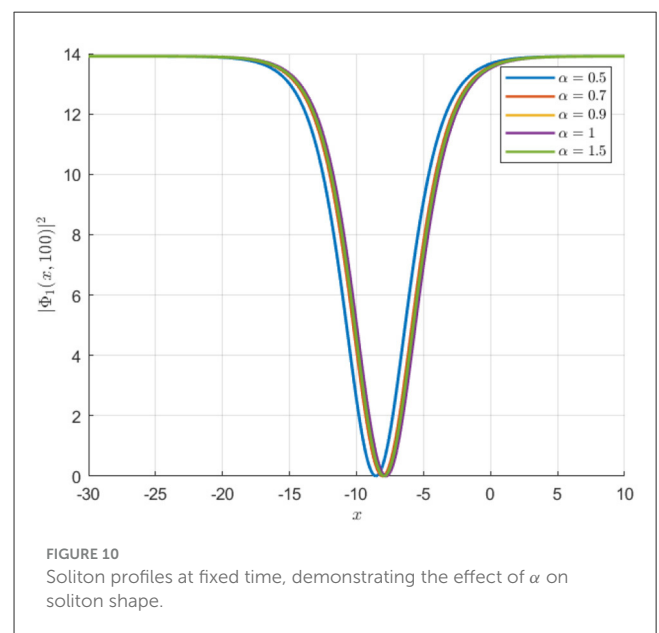
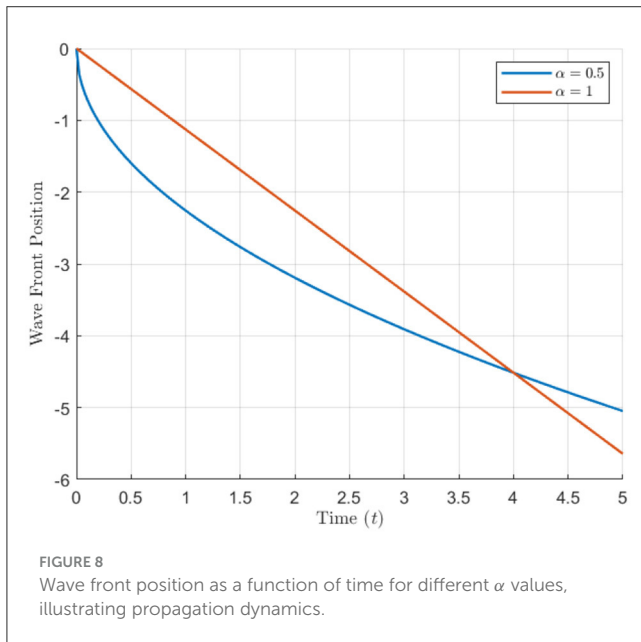
The coefficients $\varrho_3, \varrho_4, \beta_0$, and β_1 are given by the following expressions:

$$\begin{aligned} \varrho_3 &= \frac{-24\varrho_1\gamma_0^2\varrho_6 - 4\varrho_7\varrho_2\gamma_0 - \varrho_7\varrho_6 + \sqrt{-(4\varrho_7\varrho_5 - \varrho_6^2)(24\varrho_1\gamma_0^2 - \varrho_7)^2}}{2\varrho_7\gamma_0}, \\ \varrho_4 &= \frac{(-4\varrho_1\gamma_0^2 + \varrho_7)\sqrt{-(4\varrho_7\varrho_5 - \varrho_6^2)(24\varrho_1\gamma_0^2 - \varrho_7)^2} + 96\gamma_0\left(\varrho_1\gamma_0\varrho_6 + \frac{\varrho_7\varrho_2}{2}\right)\left(\varrho_1\gamma_0^2 - \frac{\varrho_7}{24}\right)}{\gamma_0\left(24\varrho_1\gamma_0^2\varrho_6 - \varrho_6\varrho_7 - \sqrt{-(4\varrho_7\varrho_5 - \varrho_6^2)(24\varrho_1\gamma_0^2 - \varrho_7)^2}\right)}, \\ \beta_0 &= 0, \end{aligned} \quad (18)$$

$$\beta_1 = \frac{\left(-2\gamma_0 \left(-24\varrho_1\gamma_0^2\varrho_6 + \varrho_7\varrho_6 \right) + \sqrt{-(4\varrho_7\varrho_5 - \varrho_6^2)(24\varrho_1\gamma_0^2 - \varrho_7)^2} \right) \varrho_7(24\varrho_1\gamma_0^2 - \varrho_7)^{\frac{1}{2}}}{\gamma_0 \left(-24\varrho_1\gamma_0^2\varrho_6 + \varrho_7\varrho_6 \right) + \sqrt{-(4\varrho_7\varrho_5 - \varrho_6^2)(24\varrho_1\gamma_0^2 - \varrho_7)^2}}.$$

Utilizing Equations 3, 8, 14, and 18, we obtain the following optical solutions:

$$\Phi_{11}(x, t) = \beta_1 \sqrt{-\gamma_0} \tanh \left(\sqrt{-\gamma_0} \left(h \left(x - \frac{\lambda_1 t^\alpha}{\alpha} \right) + s \right) \right) e^{i \left(-kx + \frac{wt^\alpha}{\alpha} + \phi \right)}, \quad (19)$$



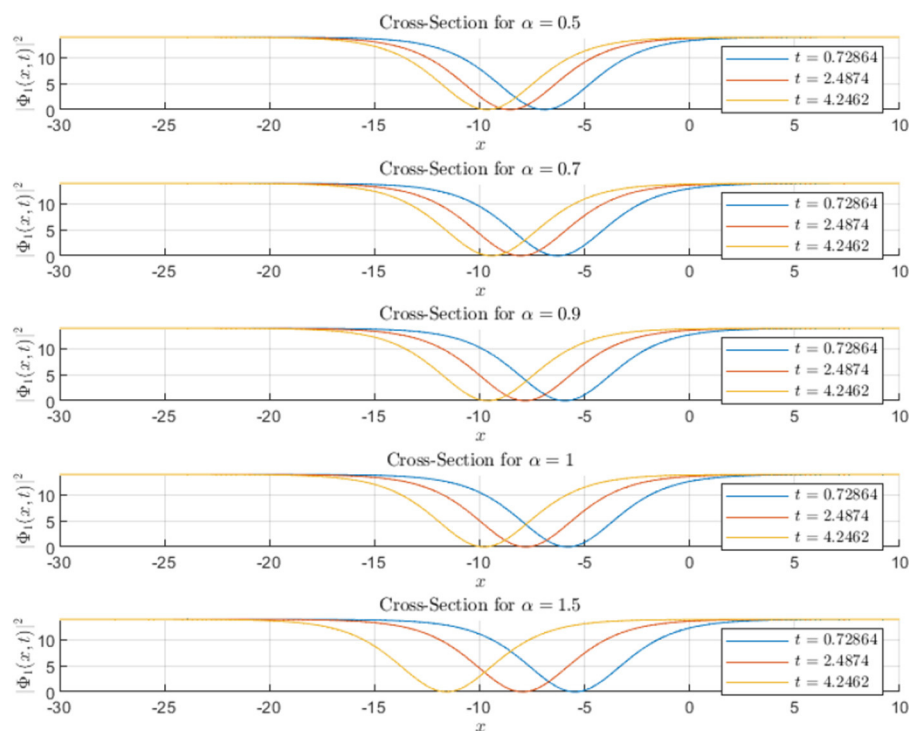


FIGURE 11
Cross-sectional view of soliton intensity $|\Phi(x, t)|^2$ for different α values.

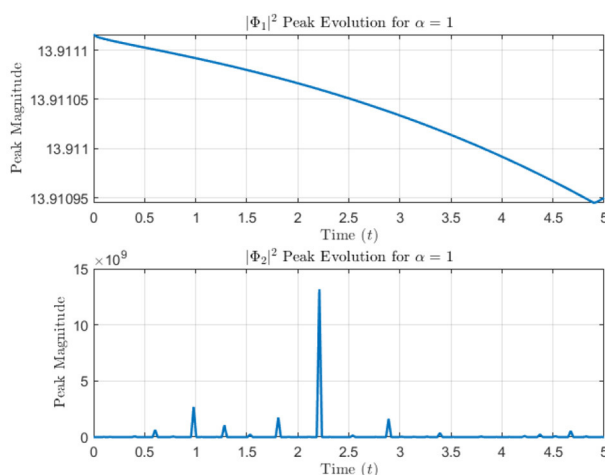


FIGURE 12
Temporal evolution of soliton wave $|\Phi(x, t)|^2$ over time, showing propagation dynamics for different α values.

$$\Phi_{12}(x, t) = \beta_1 \sqrt{-\gamma_0} \coth \left(\sqrt{-\gamma_0} \left(h \left(x - \frac{\lambda_1 t^\alpha}{\alpha} \right) + s \right) \right) e^{i \left(-kx + \frac{wt^\alpha}{\alpha} + \phi \right)}, \quad (20)$$

$$\Phi_{13}(x, t) = \beta_1 \sqrt{-\gamma_0} \left(-\tanh \left(2\sqrt{-\gamma_0} \left(h \left(x - \frac{\lambda_1 t^\alpha}{\alpha} \right) + s \right) \right) \right)$$

$$+ i \operatorname{sech} \left(2\sqrt{-\gamma_0} \left(h \left(x - \frac{\lambda_1 t^\alpha}{\alpha} \right) + s \right) \right) e^{i \left(-kx + \frac{wt^\alpha}{\alpha} + \phi \right)}, \quad (21)$$

$$\Phi_{14}(x, t) = \beta_1 \sqrt{-\gamma_0} \left(-\coth \left(2\sqrt{-\gamma_0} \left(h \left(x - \frac{\lambda_1 t^\alpha}{\alpha} \right) + s \right) \right) \right) \quad (22)$$

$$+ \operatorname{csch} \left(2\sqrt{-\gamma_0} \left(h \left(x - \frac{\lambda_1 t^\alpha}{\alpha} \right) + s \right) \right) e^{i \left(-kx + \frac{wt^\alpha}{\alpha} + \phi \right)},$$

$$\Phi_{15}(x, t) = \beta_1 \sqrt{-\gamma_0} \left(\tanh \left(\frac{\sqrt{-\gamma_0}}{2} \left(h \left(x - \frac{\lambda_1 t^\alpha}{\alpha} \right) + s \right) \right) \right) \quad (23)$$

$$+ \coth \left(\frac{\sqrt{-\gamma_0}}{2} \left(h \left(x - \frac{\lambda_1 t^\alpha}{\alpha} \right) + s \right) \right) e^{i \left(-kx + \frac{wt^\alpha}{\alpha} + \phi \right)}.$$

Additionally, applying Equations 3, 8, 14, 15, and 18 yields the following optical solutions:

$$\Phi_{16}(x, t) = \beta_1 \sqrt{\gamma_0} \tan \left(\sqrt{\gamma_0} \left(h \left(x - \frac{\lambda_1 t^\alpha}{\alpha} \right) + s \right) \right) e^{i \left(-kx + \frac{wt^\alpha}{\alpha} + \phi \right)}, \quad (24)$$

$$\Phi_{17}(x, t) = \beta_1 \sqrt{\gamma_0} \cot \left(\sqrt{\gamma_0} \left(h \left(x - \frac{\lambda_1 t^\alpha}{\alpha} \right) + s \right) \right) e^{i \left(-kx + \frac{wt^\alpha}{\alpha} + \phi \right)}, \quad (25)$$

$$\Phi_{18}(x, t) = \beta_1 \sqrt{\gamma_0} \left(-\tan \left(2\sqrt{\gamma_0} \left(h \left(x - \frac{\lambda_1 t^\alpha}{\alpha} \right) + s \right) \right) + \sec \left(2\sqrt{\gamma_0} \left(h \left(x - \frac{\lambda_1 t^\alpha}{\alpha} \right) + s \right) \right) \right) e^{i \left(-kx + \frac{wt^\alpha}{\alpha} + \phi \right)}, \quad (26)$$

$$\Phi_{19}(x, t) = \beta_1 \sqrt{\gamma_0} \left(-\cot \left(2\sqrt{\gamma_0} \left(h \left(x - \frac{\lambda_1 t^\alpha}{\alpha} \right) + s \right) \right) + \csc \left(2\sqrt{\gamma_0} \left(h \left(x - \frac{\lambda_1 t^\alpha}{\alpha} \right) + s \right) \right) \right) e^{i \left(-kx + \frac{wt^\alpha}{\alpha} + \phi \right)}, \quad (27)$$

$$\Phi_{20}(x, t) = \beta_1 \sqrt{\gamma_0} \left(\tan \left(\frac{\sqrt{\gamma_0}}{2} \left(h \left(x - \frac{\lambda_1 t^\alpha}{\alpha} \right) + s \right) \right) + \cot \left(\frac{\sqrt{\gamma_0}}{2} \left(h \left(x - \frac{\lambda_1 t^\alpha}{\alpha} \right) + s \right) \right) \right) e^{i \left(-kx + \frac{wt^\alpha}{\alpha} + \phi \right)}. \quad (28)$$

The following figures present various aspects of soliton solutions $\Phi_{11}(x, t)$ for two different values of the fractional-order parameter $\alpha = 0.5$ and $\alpha = 1.5$. The simulations are based on the following parameters:

$$\begin{aligned} a &= -0.9, & b &= 0.2, & w &= 2, \\ \tau_1 &= 0.1, & \tau_3 &= 0.1, & \tau_4 &= 0.5, \\ \tau_5 &= 0.5, & \tau_6 &= 0.5, & \tau_7 &= 0.7, \\ \tau_8 &= 1, & \tau_9 &= 2, & h &= 0.1, \\ c_1 &= 0.1, & c_2 &= 0.1, & \gamma_0 &= -10, \\ \phi &= 0.1, & s &= 0.5. \end{aligned}$$

The results are presented for different values of the fractional order parameter α .

The figures provide a comparative analysis of soliton intensity, spatial profiles, peak magnitudes, and wave front dynamics. The results demonstrate the influence of varying α on the dynamics and shape of the solitons. As shown in Figure 13, the soliton intensity $|\Phi_{11}(x, t)|^2$ varies with α . For $\alpha = 0.5$, the soliton maintains a broader profile, indicating slower propagation. In contrast, at $\alpha = 1.5$, the soliton exhibits a sharper, faster-evolving profile. Figure 14 highlights the spatial profile of Φ_{11} at a fixed time. The soliton for $\alpha = 1.5$ is narrower and shifts forward compared to $\alpha = 0.5$. This indicates that higher α accelerates the soliton's evolution and alters its spatial localization. Figure 15 shows how the peak magnitude evolves over time. For $\alpha = 0.5$, the peak stabilizes slowly, while for $\alpha = 1.5$, the soliton reaches its peak faster. This reflects the faster temporal evolution of solitons at higher α . Figure 16 illustrates the propagation of the soliton wave front over time. For $\alpha = 1.5$, the wave front progresses more rapidly compared to $\alpha = 0.5$, indicating enhanced soliton mobility and faster response to perturbations. These results demonstrate that the fractional parameter α significantly affects the soliton's propagation speed, spatial profile, and peak intensity. Higher values of α lead to faster, more localized solitons, while lower α values result in broader, slower-moving solitons.

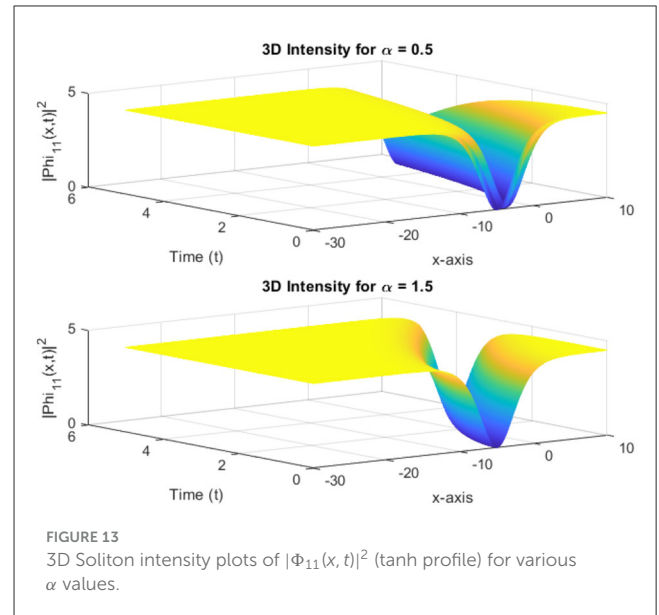


FIGURE 13
3D Soliton intensity plots of $|\Phi_{11}(x, t)|^2$ (tanh profile) for various α values.

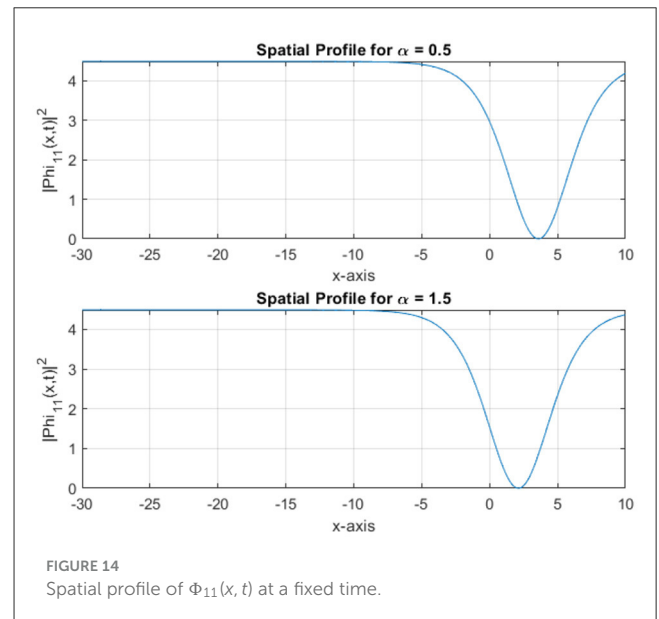
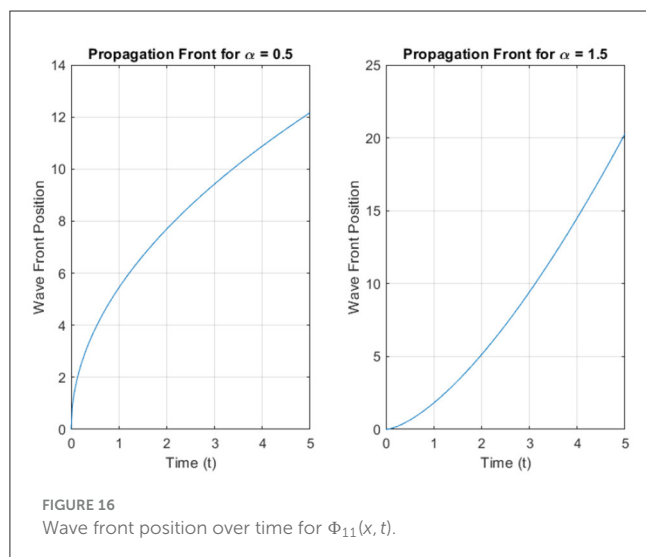
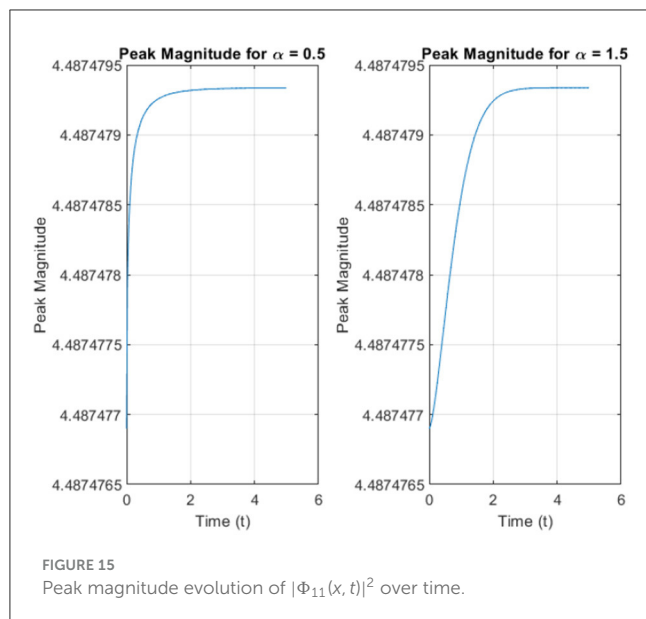


FIGURE 14
Spatial profile of $\Phi_{11}(x, t)$ at a fixed time.

5 Application of the Kudryashov method

5.1 Kudryashov method

The Kudryashov method is a powerful and efficient analytical approach for deriving exact solutions to nonlinear differential equations, particularly in the context of soliton theory and wave propagation [43]. This method has been widely applied to nonlinear evolution equations, offering explicit forms of soliton solutions that are crucial for understanding complex dynamical systems. In this section, we employ the Kudryashov method to obtain new conformable optical soliton solutions for the concatenated nonlinear model, providing deeper insights into the propagation of solitons in optical fibers.



The Kudryashov method is a systematic approach for deriving exact solutions to nonlinear differential equations. The process begins by formulating the governing nonlinear equation and applying a traveling wave transformation, typically $\xi = h(x - \frac{v\alpha}{\alpha})$, to reduce the partial differential equation (PDE) to an ordinary differential equation (ODE). An ansatz is then assumed for the solution, often in the form $\Phi(\xi) = \eta_0 + \sum_{i=1}^N \eta_i \chi^i(\xi)$, where $\chi(\xi)$ is a known function, such as a hyperbolic or trigonometric function. To determine the expansion degree N , the balancing principle is applied, equating the highest-order derivative term with the dominant nonlinear term in the equation. The assumed solution is substituted into the reduced ODE, leading to a polynomial equation in terms of $\chi(\xi)$. By collecting like terms and setting the coefficients of each power of $\chi(\xi)$ to zero, a system of algebraic equations is obtained. Solving this system provides the unknown constants (η_i, k , etc.), which are then used to construct the explicit soliton solutions. These solutions are further analyzed and

visualized to examine soliton dynamics, stability, and propagation characteristics. The method also allows for the evaluation of physical properties such as energy, peak intensity, and interaction behaviors, offering deeper insights into the complex dynamics of soliton systems.

The following solution, applicable to this model, is adopted from [44]:

$$\chi(\xi) = \frac{1}{(c_1 - c_2) \sinh(\xi) + (c_1 + c_2) \cosh(\xi)}, \quad (29)$$

where c_1 and c_2 are arbitrary constants that can be tuned to satisfy the boundary conditions and the constraints of the governing nonlinear equation. This function represents a general form of solitary wave solutions that exhibit localized behavior over an extended spatial domain [45]. The function $\chi(\xi)$ satisfies the following fundamental relation:

$$\left(\frac{d\chi(\xi)}{d\xi} \right)^2 = \chi(\xi)^2 (1 - 4c_1c_2\chi(\xi)^2). \quad (30)$$

Equation 30 highlights the nonlinearity inherent in the system, which governs the shape and amplitude of solitons. This quadratic relationship implies that the soliton amplitude is influenced by the interaction between the coefficients c_1 and c_2 , making it possible to control the soliton profile through these adjustable parameters.

To construct explicit soliton solutions to Equation 9, we adopt the following series representation using the Kudryashov approach:

$$\Phi(\xi) = \eta_0 + \sum_{i=1}^N \eta_i \chi^i(\xi), \quad (31)$$

where $\eta_0, \eta_1, \dots, \eta_N$ are unknown constants that need to be determined. The parameter N denotes the highest power of $\chi(\xi)$ in the series expansion and is determined by balancing the highest-order derivative term and the nonlinear term in the governing equation. This series form enables the extraction of various soliton profiles by solving a system of algebraic equations for the coefficients η_i .

This procedure results in a system of algebraic equations as follows:

$$\begin{aligned} (\chi(\xi))^0 &: 384c_1^2c_2^2\rho_1\beta_1 - 8c_1c_2\rho_2\beta_1^3 - 4c_1c_2\rho_3\beta_1^3 + \rho_5\beta_1^5 = 0, \\ (\chi(\xi))^1 &: -16c_1c_2\rho_2\beta_0\beta_1^2 - 4c_1c_2\rho_3\beta_0\beta_1^2 + 5\rho_5\beta_0\beta_1^4 = 0, \\ (\chi(\xi))^2 &: -8c_1c_2\rho_2\beta_0^2\beta_1 + 10\rho_5\beta_0^2\beta_1^3 - 8c_1c_2\rho_1\beta_1 - 8c_1c_2\rho_1\beta_1 \\ &\quad + (\rho_2 + \rho_3 + \rho_6)\beta_1^3 = 0, \\ (\chi(\xi))^3 &: 10\rho_5\beta_0^3\beta_1^2 + 2\rho_2\beta_0\beta_1^2 + \rho_3\beta_0\beta_1^2 + 3\rho_6\beta_0\beta_1^2 = 0, \\ (\chi(\xi))^4 &: 5\rho_5\beta_0^4\beta_1 + \rho_2\beta_0^2\beta_1 + 3\rho_6\beta_0^2\beta_1 + (\rho_1 + \rho_4 + \rho_7)\beta_1 = 0, \\ (\chi(\xi))^5 &: \rho_5\beta_0^5 + \rho_6\beta_0^3 + \rho_7\beta_0 = 0. \end{aligned} \quad (32)$$

Once again, two cases can be considered. First case: The solutions to the above system are given by:

$$\begin{aligned}\rho_1 &= -\rho_4 - \rho_7, \\ \rho_5 &= \frac{3 \left((-\rho_2 + \frac{\rho_3}{2} + 2\rho_6) \rho_4 + 4\rho_7 \left(-\rho_2 + \frac{\rho_3}{3} + \frac{3\rho_6}{2} \right) \right)}{(9\rho_4 + 10\rho_7)^2}, \\ \beta_0 &= 0, \\ \beta_1 &= -\frac{2\sqrt{-2(\rho_2 + \rho_3 + \rho_6)} c_1 c_2 (9\rho_4 + 10\rho_7)}{\rho_2 + \rho_3 + \rho_6}.\end{aligned}\quad (33)$$

Using Equations 4, 5, 8, and 33, the following optical solutions are derived

$$\begin{aligned}\Phi_{21}(x, t) &= \frac{\beta_1 e^{i(-kx + \frac{wt^\alpha}{\alpha} + \phi)}}{(c_1 - c_2) \sinh \left(h \left(x - \frac{\lambda_1 t^\alpha}{\alpha} \right) \right) + (c_1 + c_2) \cosh \left(h \left(x - \frac{\lambda_1 t^\alpha}{\alpha} \right) \right)}, \\ \Phi_{22}(x, t) &= \frac{\beta_1}{2c_2} \operatorname{sech} \left(h \left(x - \frac{\lambda_1 t^\alpha}{\alpha} \right) \right) e^{i(-kx + \frac{wt^\alpha}{\alpha} + \phi)}, \\ \Phi_{23}(x, t) &= -\frac{\beta_1}{2c_2} \operatorname{csch} \left(h \left(x - \frac{\lambda_1 t^\alpha}{\alpha} \right) \right) e^{i(-kx + \frac{wt^\alpha}{\alpha} + \phi)}.\end{aligned}\quad (34)$$

A second case can be considered: The solutions to the algebraic system yield the following expressions:

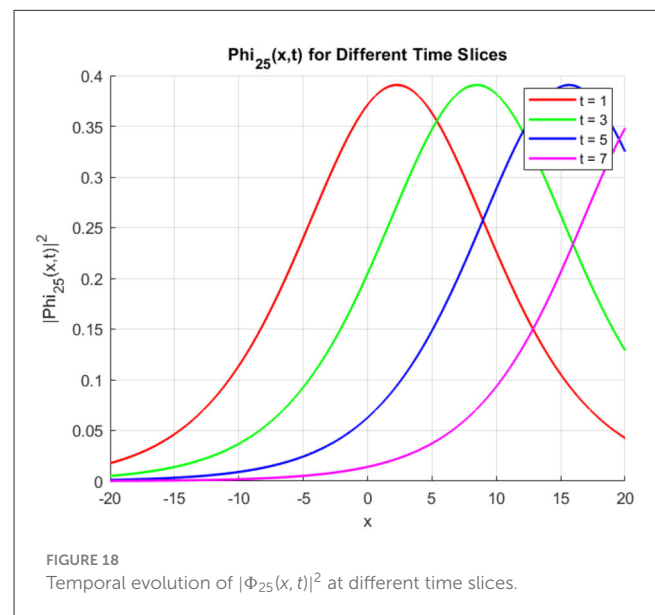
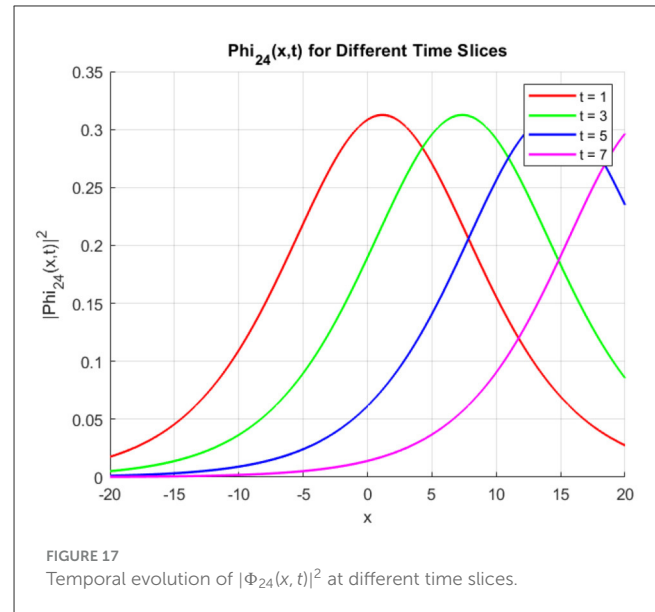
$$\begin{aligned}\rho_4 &= -\rho_7 - \rho_1, \\ \rho_5 &= \frac{3(\rho_6 + \rho_2 + \rho_3) \left((\rho_2 - \frac{\rho_3}{2} - 2\rho_6) \rho_1 - \rho_7 (\rho_2 + \frac{\rho_3}{3}) \right)}{(9\rho_1 - \rho_7)^2}, \\ \beta_0 &= 0, \\ \beta_1 &= \frac{2\sqrt{2(\rho_6 + \rho_2 + \rho_3)} c_1 c_2 (9\rho_1 - \rho_7)}{\rho_6 + \rho_2 + \rho_3}.\end{aligned}\quad (35)$$

Utilizing Equations 4, 5, 8, and 35, the following optical solutions are derived:

$$\begin{aligned}\Phi_{24}(x, t) &= \frac{\beta_1 e^{i(-kx + \frac{wt^\alpha}{\alpha} + \phi)}}{(c_1 - c_2) \sinh \left(h \left(x - \frac{\lambda_1 t^\alpha}{\alpha} \right) \right) + (c_1 + c_2) \cosh \left(h \left(x - \frac{\lambda_1 t^\alpha}{\alpha} \right) \right)}, \\ \Phi_{25}(x, t) &= \frac{\beta_1}{2c_2} \operatorname{sech} \left(h \left(x - \frac{\lambda_1 t^\alpha}{\alpha} \right) \right) e^{i(-kx + \frac{wt^\alpha}{\alpha} + \phi)}, \\ \Phi_{26}(x, t) &= -\frac{\beta_1}{2c_2} \operatorname{csch} \left(h \left(x - \frac{\lambda_1 t^\alpha}{\alpha} \right) \right) e^{i(-kx + \frac{wt^\alpha}{\alpha} + \phi)}.\end{aligned}\quad (36)$$

5.2 Visualization and analysis of soliton dynamics

Figure 17 displays the time evolution of $|\Phi_{24}(x, t)|^2$ for four distinct time slices ($t = 1, 3, 5, 7$). The soliton maintains a smooth bell-shaped profile as it propagates in the positive x -direction. The peak intensity gradually decreases, and the soliton broadens slightly over time, indicating a stable, spreading wave. The curve shifts



rightward, highlighting the directional propagation of the wave. Figure 18 illustrates the evolution of $|\Phi_{25}(x, t)|^2$, where the soliton retains a bright, localized peak as it propagates. The peak remains nearly constant in intensity, a characteristic of bright solitons. Over time, the soliton maintains its structure while moving along the positive x -axis, demonstrating its robustness and stability. Figure 19 presents the evolution of $|\Phi_{26}(x, t)|^2$, which features sharp peaks caused by the singularity of the csch function. The soliton exhibits high-intensity spikes at different time steps, with the peaks shifting rightward as time progresses. The peak intensities are significantly larger compared to Φ_{24} and Φ_{25} , highlighting the soliton's distinct singular nature. Figure 20 illustrates the logarithmic peak intensity evolution of the soliton solutions Φ_{24} , Φ_{25} , and Φ_{26} over time. All the figures presented were generated using the parameter values listed in Table 1.

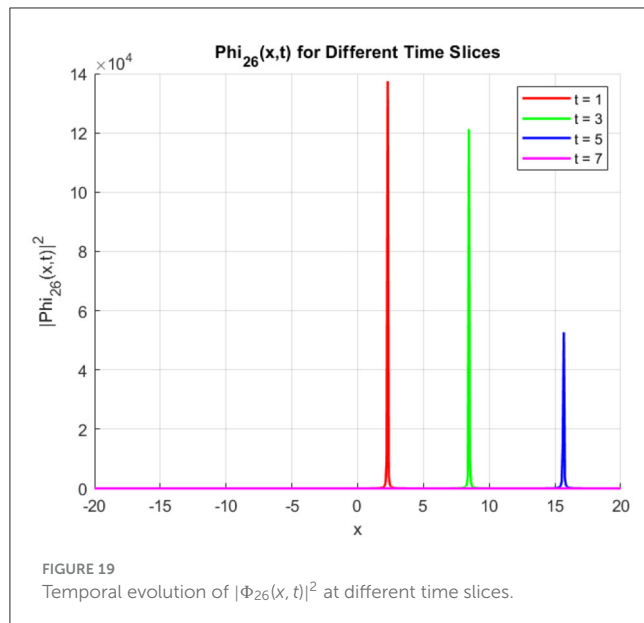


FIGURE 19
Temporal evolution of $|\Phi_{26}(x,t)|^2$ at different time slices.

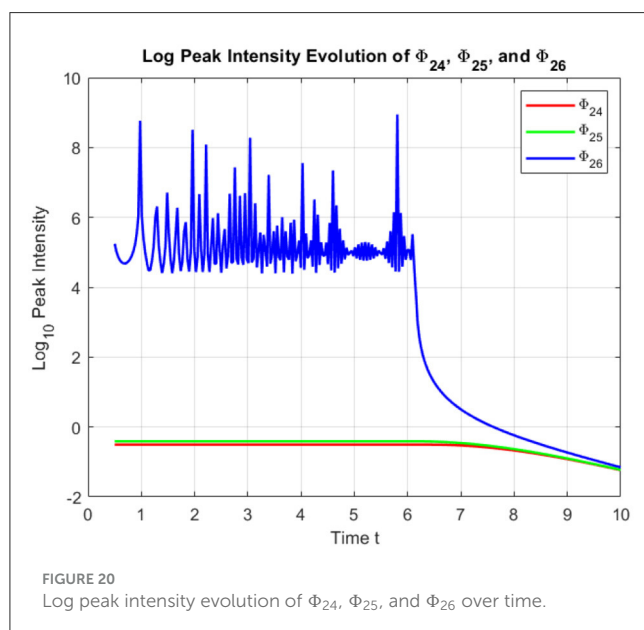


FIGURE 20
Log peak intensity evolution of Φ_{24} , Φ_{25} , and Φ_{26} over time.

The soliton solutions Φ_{24} and Φ_{25} maintain stable peak intensities throughout their evolution, exhibiting only minimal decay over time. This behavior highlights their inherent stability as soliton structures, making them resilient to dispersive and nonlinear effects. In contrast, Φ_{26} displays pronounced high-intensity spikes and irregular fluctuations, a hallmark of singular solutions driven by the hyperbolic cosecant function embedded in its formulation. These sharp intensity variations reflect its susceptibility to rapid amplitude changes. Notably, after $t = 6$, Φ_{26} experiences a rapid decay in energy, leading to a transition into a lower energy state. This post-peak energy loss further emphasizes the transient and unstable nature of Φ_{26} compared to the more stable profiles of Φ_{24} and Φ_{25} .

5.3 Multi-soliton interactions and collisions

We analyzed the structural relationships in soliton interactions and examined their properties. This part delves into the interaction dynamics between two distinct soliton solutions, namely the Sech-based soliton Φ_{25} and the Csch-based soliton Φ_{26} , derived using the Kudryashov method. These soliton solutions exhibit distinct characteristics: Φ_{25} is known for its localized and stable bell-shaped profile, while Φ_{26} introduces a singular behavior due to its hyperbolic cosecant structure [46].

The interaction between solitons is modeled here via linear superposition of two exact solutions (Φ_{25} and Φ_{26}). While this approach does not yield a true multi-soliton solution, it offers a tractable approximation for non-integrable systems. Notably, Equation 1 contains non-variational terms involving Φ^* , precluding a Lagrangian formulation and thus the use of action-based interaction analysis. The superposition method is therefore used as a qualitative tool to capture essential features of soliton dynamics such as amplitude modulation and energy redistribution.

The combined soliton solution for the multi-soliton interaction is constructed by superimposing the two solitons:

$$\Phi_{\text{total}}(x,t) = \Phi_{25}(x,t) + \Phi_{26}(x,t), \quad (37)$$

where

$$\Phi_{25}(x,t) = \frac{\beta_1}{2c_2} \text{sech} \left(h \left(x - \frac{\lambda_1 t^\alpha}{\alpha} \right) \right) e^{i(-kx + \frac{wt^\alpha}{\alpha} + \phi)}, \quad (38)$$

and

$$\Phi_{26}(x,t) = -\frac{\beta_1}{2c_2} \text{csch} \left(h \left(x - \frac{\lambda_1 t^\alpha}{\alpha} \right) \right) e^{i(-kx + \frac{wt^\alpha}{\alpha} + \phi)}. \quad (39)$$

The interaction between Φ_{25} and Φ_{26} reveals complex dynamics driven by the interplay of the hyperbolic secant and cosecant functions, leading to energy exchange, intensity fluctuations, and non-trivial collision behavior.

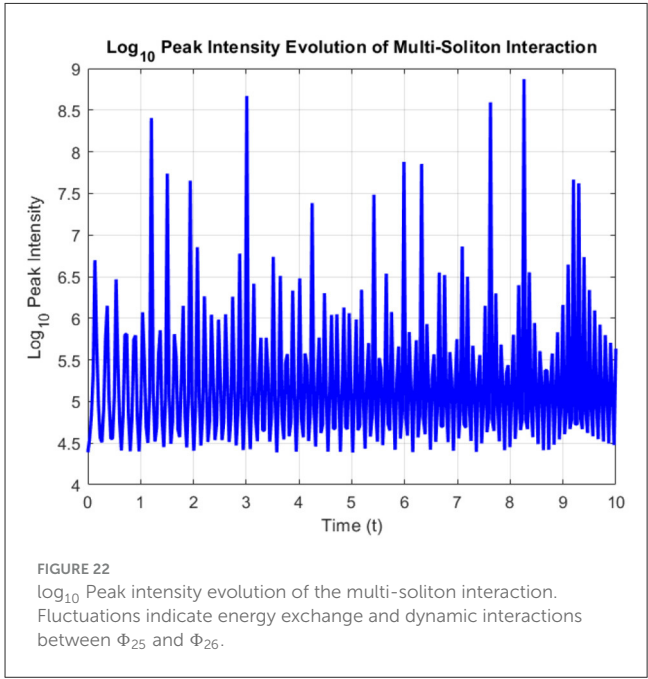
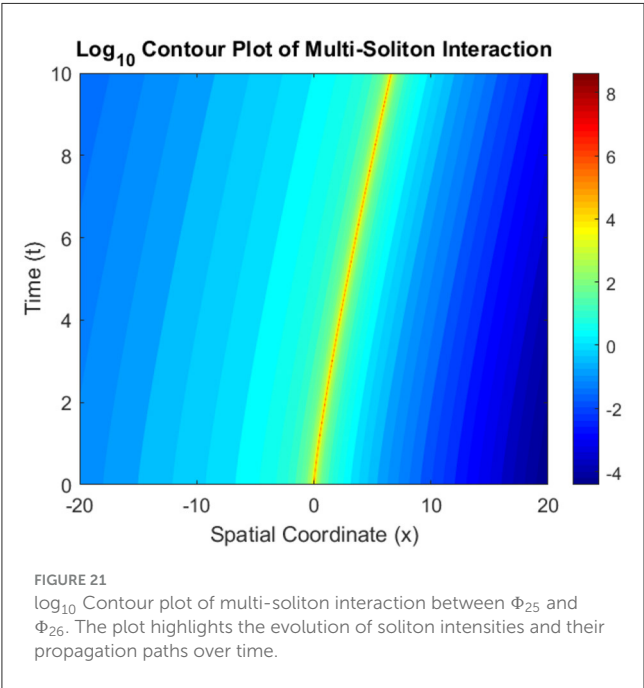
Figure 21 presents the log₁₀ contour plot of the combined soliton interaction over time and space. The color gradient effectively visualizes the soliton trajectories and intensity variations. The Sech-based soliton (Φ_{25}) contributes a smooth, bell-shaped trajectory, while the Csch-based soliton (Φ_{26}) introduces sharp gradients and localized spikes due to its singular nature.

The contour plot illustrates the propagation of solitons over the spatial domain, with visible energy exchanges during interactions. High-intensity regions are marked in warmer colors, while regions of lower intensity are displayed in cooler tones. The log scale enhances the visualization of both strong and weak intensity regions.

To further analyze the interaction dynamics, Figure 22 displays the evolution of the peak intensity over time on a logarithmic scale. The plot captures the oscillatory behavior of the intensity peaks, reflecting energy fluctuations during the interaction process. The logarithmic scale highlights subtle variations and abrupt intensity spikes. The observed fluctuations are characteristic of the

TABLE 1 Parameters used to generate all figures in the Kudryashov method, including the log peak intensity plot.

Parameter	Symbol	Value	Parameter	Symbol	Value
Chromatic dispersion	a	-0.9	Higher dispersion	τ_7	0.7
Kerr nonlinearity	b	0.2	Nonlinear interaction	τ_8	1
Angular frequency	w	2	Nonlinear interaction	τ_9	2
Dispersion term	τ_1	0.1	Scaling factor	h	0.1
Nonlinearity term	τ_3	0.1	Coefficient 1	c_1	0.1
Self-Phase modulation	τ_4	0.5	Coefficient 2	c_2	0.1
Nonlinear term	τ_5	0.5	Fractional derivative	α	1.2
Fifth-Order term	τ_6	0.5	Arbitrary constant	ϕ	0.1
Conformable parameter	s	0.5	Scaling constant	c_1	1
Scaling constant	c_2	0.8	Conformal derivative	γ_0	-10
Amplitude factor	β_1	1			



interaction between stable and singular soliton structures, where transient energy surges occur at collision points.

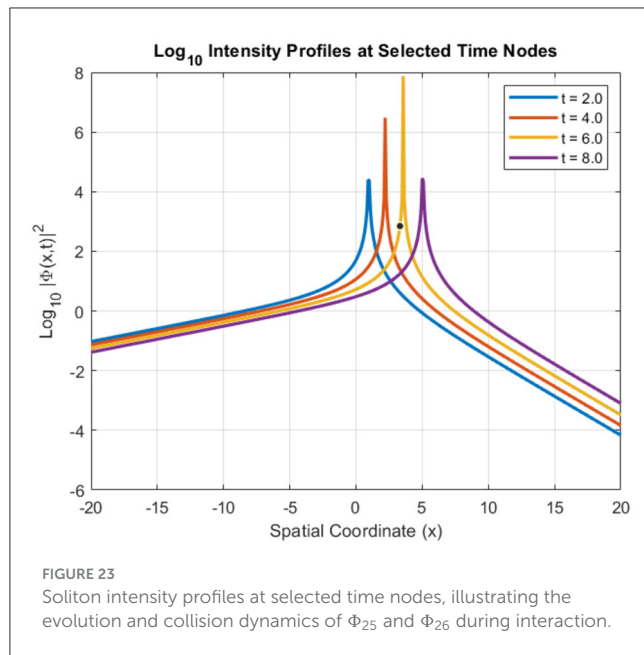
To provide a clearer and more concise understanding of soliton evolution, Figure 23 presents intensity profiles at specific time slices, revealing how the spatial structures of the solitons Φ_{25} and Φ_{26} evolve during their interaction. These snapshots depict the dynamic nature of the soliton profiles, showcasing key phenomena such as energy exchange, stability, and collision dynamics. The interaction between the sech-based soliton Φ_{25} and the csch-based soliton Φ_{26} demonstrates transient energy redistribution, where peak intensities undergo periodic amplification and suppression.

Notably, Φ_{25} retains structural stability despite the interaction, while Φ_{26} exhibits significant fluctuations due to its inherent singular characteristics. During collision events, sharp intensity

spikes are observed, followed by the gradual restoration of each soliton's original profile, reflecting the hallmark elastic behavior of soliton interactions. The contrasting behaviors of these two soliton types result in complex nonlinear dynamics. Φ_{25} displays localized energy concentration and stable propagation, making it ideal for applications that demand signal consistency. In contrast, Φ_{26} undergoes rapid intensity shifts and strong localization effects, which are commonly observed in singular soliton dynamics and have implications in fields such as plasma physics and hydrodynamics.

The logarithmic intensity analysis provides deeper insight into both dominant and subtle features, capturing energy fluctuations across strong and weak regions within the system.

To quantify these interactions, the total energy of the system is computed using the expression:

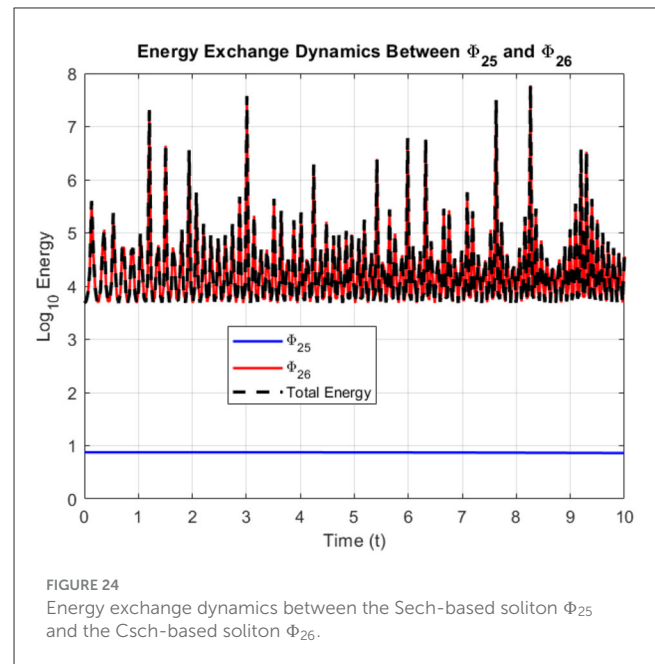


$$E(t) = \int_{-\infty}^{\infty} |\Phi_{25}(x, t) + \Phi_{26}(x, t)|^2 dx,$$

where $\Phi_{25}(x, t)$ and $\Phi_{26}(x, t)$ represent the individual soliton waveforms, and $|\Phi(x, t)|^2$ corresponds to the soliton intensity. Expanding the square modulus gives:

$$E(t) = \int_{-\infty}^{\infty} (|\Phi_{25}(x, t)|^2 + |\Phi_{26}(x, t)|^2 + 2\Re[\Phi_{25}(x, t)\Phi_{26}^*(x, t)]) dx,$$

where the total energy includes contributions from each soliton and an interaction term reflecting interference effects. The energy dynamics were calculated numerically using the trapezoidal rule for spatial integration, with the results plotted over time on a logarithmic scale (\log_{10}) to highlight fluctuations and ensure clear visibility of energy variations. The energy evolution, illustrated in Figure 24, reveals distinct patterns for the two solitons. The Sech-based soliton Φ_{25} maintains a stable energy profile, indicating its robustness against interaction-induced perturbations. In contrast, the CsCh-based soliton Φ_{26} undergoes frequent energy spikes and fluctuations, a direct consequence of its singular nature. Despite these localized changes, the total energy of the system remains largely conserved, adhering to the principles of integrable systems where energy conservation is a fundamental characteristic. This conservation persists even during intense soliton interactions, underscoring the stability of the system. The energy exchange between the solitons highlights how transient redistributions occur without violating global conservation laws. Such behavior is pivotal in understanding energy transfer mechanisms in nonlinear media, with practical applications in optical communication, fluid dynamics, and plasma physics. The combined analysis of intensity evolution and energy dynamics emphasizes the diverse behaviors that arise from the interaction of Sech-based and CsCh-based



solitons. It also showcases the effectiveness of fractional calculus in modeling complex soliton systems, enabling the accurate depiction of nonlinear interactions, stability considerations, and energy conservation. These insights not only deepen the theoretical understanding of soliton behavior but also pave the way for future explorations in applied fields where soliton dynamics play a critical role.

6 Conclusion

This study presents a comprehensive analysis of multi-soliton dynamics within a conformable concatenated nonlinear model, integrating the nonlinear Schrödinger equation (NLSE), the Sasa-Satsuma (SS) equation, and the Lakshmanan-Porsezian-Daniel (LPD) model. Through the application of advanced analytical techniques—specifically, the modified simplest equation method and the Kudryashov approach—a wide array of exact soliton solutions was systematically derived, including bright, dark, and mixed types. These solutions offer valuable insights into the complex interplay between higher-order dispersion and nonlinear effects, which strongly affect soliton stability, propagation dynamics, and spatial evolution in optical fibers.

A key contribution of this research lies in the incorporation of a conformable fractional derivative, which significantly extends the analytical scope of the model. This fractional framework enables precise and accurate modeling of fractional-order dynamics, capturing intricate behaviors such as energy dissipation, temporal evolution, and soliton stability under varying system parameters. The study reveals how small variations in the fractional order significantly alter soliton profiles, peak intensities, and interaction dynamics, thereby enhancing the flexibility and depth of soliton analysis.

The energy dynamics of soliton interactions were also meticulously examined, emphasizing both individual soliton

energies and the total system energy. Using numerical integration techniques, it was demonstrated that—despite complex interaction events such as elastic and inelastic collisions—the total energy of the system remains largely conserved. This observation reflects a fundamental property of soliton systems within integrable models, demonstrating that localized fluctuations do not disrupt overall energy conservation. The application of a logarithmic scale in visualizations further confirmed these fluctuations while reinforcing conservation principles.

Numerical simulations validated the analytical solutions and illustrated how temporal and fractional parameters influence soliton dynamics, peak intensities, and propagation behaviors. Comparative analysis between sech- and csch-based solitons revealed rich nonlinear phenomena, including energy exchange, amplitude modulation, and collision-induced structural changes. In particular, the energy stability of sech-based solitons contrasted with the pronounced fluctuations of csch-based solitons, providing valuable insight into the diverse dynamics governing nonlinear wave systems.

The insights gained from this study not only deepen the understanding of nonlinear wave dynamics but also pave the way for the development of next-generation telecommunication systems. The ability to model, predict, and control soliton behavior with high precision holds immense potential to enhance data transmission efficiency, reduce signal degradation, and optimize optical network infrastructures. Ultimately, the integration of fractional calculus into soliton research opens new avenues for the exploration of complex nonlinear systems across diverse scientific fields, including fluid dynamics, plasma physics, and quantum mechanics.

Data availability statement

The original contributions presented in the study are included in the article/supplementary material, further inquiries can be directed to the corresponding author.

References

1. Yoshida S. Physics and mathematics behind wave dynamics. In: *Synthesis Lectures on Wave Phenomena in the Physical Sciences*. Cham, Switzerland: Springer. (2025). doi: 10.1007/978-3-031-60354-9
2. Chen YQ, Tang YH, Manafian J, Rezazadeh H, Osman MS. Dark wave, rogue wave and perturbation solutions of Ivancevic option pricing governing model. *Nonlinear Dyn.* (2021) 105:2539–48. doi: 10.1007/s11071-021-06642-6
3. Raza N, Rani B, Chahlaoui Y, Shah NA, A. variety of new rogue wave patterns for three coupled nonlinear Maccari's models in complex form. *Nonlinear Dyn.* (2023) 111:18419–37. doi: 10.1007/s11071-023-08839-3
4. Jhangeer A, Ansari AR, Imran M, Riaz MB, Talafha AM. Application of propagating solitons to Ivancevic option pricing governing model and construction of first integral by Nucci's direct reduction approach. *Ain Shams Eng J.* (2024) 15:102615. doi: 10.1016/j.asej.2023.102615
5. Ahmed KK, Badra NM, Ahmed HM, Rabie WB. Unveiling optical solitons and other solutions for fourth-order (2+1)-dimensional nonlinear Schrödinger equation by modified extended direct algebraic method. *J Opt.* (2024) 2024:1–13. doi: 10.1007/s12596-024-01690-8
6. Iqbal M, Seadawy AR, Lu D, Zhang Z. Multiple optical soliton solutions for wave propagation in nonlinear low-pass electrical transmission lines under analytical approach. *Opt Quantum Electron.* (2024) 56:35. doi: 10.1007/s11082-024-06664-5
7. Kukkar A, Kumar S, Malik S, Murad MAS, Arnous AH, Biswas A, et al. Lie symmetry analysis of cubic quartic optical solitons having cubic quantic septic nonic form of self-phase modulation structure. *J Opt.* 2024;p. 1–11. doi: 10.1007/s12596-024-01922-x
8. Manukure S, Booker T, A. short overview of solitons and applications. *Partial Differ Equation Appl Math.* (2021) 4:100140. doi: 10.1016/j.padiff.2021.100140
9. Li Z, Huang C, Wang B. Phase portrait, bifurcation, chaotic pattern and optical soliton solutions of the Fokas-Lenells equation with cubic-quartic dispersion in optical fibers. *Phys Lett A.* (2023) 465:128714. doi: 10.1016/j.physleta.2023.128714
10. Mathanarajan T, Kumar D, Rezazadeh H, Akinyemi I. Optical solitons in metamaterials with third and fourth order dispersions. *Opt Quantum Electron.* (2022) 55:271. doi: 10.1007/s11082-022-03656-1
11. Iqbal M, Seadawy AR, Lu D, Zhang Z. Physical structure and multiple solitary wave solutions for the nonlinear Jaulent-Miodek hierarchy equation. *Mod Phys Lett B.* (2023) 28:2341016. doi: 10.1142/S0217984923410166
12. Mathanarajan T. Optical soliton, linear stability analysis and conservation laws via multipliers to the integrable Kuralay equation. *Optik (Stuttg).* (2023) 290:171266. doi: 10.1016/j.ijleo.2023.171266

Author contributions

CC: Formal analysis, Methodology, Software, Writing – original draft. SA: Investigation, Methodology, Validation, Writing – original draft, Writing – review & editing. DA: Formal analysis, Supervision, Validation, Writing – original draft, Writing – review & editing.

Funding

The author(s) declare that no financial support was received for the research and/or publication of this article.

Conflict of interest

The authors declare that the research was conducted in the absence of any commercial or financial relationships that could be construed as a potential conflict of interest.

Generative AI statement

The author(s) declare that no Gen AI was used in the creation of this manuscript.

Publisher's note

All claims expressed in this article are solely those of the authors and do not necessarily represent those of their affiliated organizations, or those of the publisher, the editors and the reviewers. Any product that may be evaluated in this article, or claim that may be made by its manufacturer, is not guaranteed or endorsed by the publisher.

13. Bekir A, Raza N, Rezazadeh H, Rafiq MH. Optical Solitons of the (2+1)-Dimensional Kundu-Mukherjee-Naskar Equation with Lokal M-Derivative. *Authorea*. (2022). doi: 10.22541/au.164864681.13404176/v1
14. Kudryashov NA. One method for finding exact solutions of nonlinear differential equations. *Commun Nonlinear Sci Numer Simul*. (2012) 17:2248–53. doi: 10.1016/j.cnsns.2011.10.016
15. Podder A, Arefin MA, Akbar MA, Uddin MH. A study of the wave dynamics of the space-time fractional nonlinear evolution equations of beta derivative using the improved Bernoulli sub-equation function approach. *Sci Rep*. (2023) 13:20478. doi: 10.1038/s41598-023-45423-6
16. Murad MAS, Faridi WA, Iqbal M, Arnous AH, Shah NA, Chung JD. Analysis of Kudryashov's equation with conformable derivative via the modified Sardar sub-equation algorithm. *Results Phys*. (2024) 60:107678. doi: 10.1016/j.rinp.2024.107678
17. Zaman UHM, Arefin MA, Akbar MA, Uddin MH. Utilizing the extended tanh-function technique to scrutinize fractional order nonlinear partial differential equations. *Partial Differ Equations Appl Math*. (2023) 8:100563. doi: 10.1016/j.padiff.2023.100563
18. Soliman M, Ahmed HM, Badra N, Samir I. Effects of fractional derivative on fiber optical solitons of (2+1) perturbed nonlinear Schrödinger equation using improved modified extended tanh-function method. *Opt Quantum Electron*. (2024) 56:777. doi: 10.1007/s11082-024-06593-3
19. Zhang L, Shen B, Jia M, Wang Z, Wang G. Fractional Consistent Riccati Expansion Method and Soliton-Cnoidal Solutions for the Time-Fractional Extended Shallow Water Wave Equation in (2+1)-Dimension. *Fractals*. (2024) 8:599. doi: 10.3390/fractalfract8100599
20. Kumar S, Niwas M. New optical soliton solutions of Biswas Arshed equation using the generalised exponential rational function approach and Kudryashov's simplest equation approach. *Pramana*. (2022) 96:204. doi: 10.1007/s12043-022-02450-8
21. Ozkan YS, Yasar E. Prolific new M-fractional soliton behaviors to the Schrödinger type Ivancevic option pricing model by two efficient techniques. *Comput Methods Differ Equations*. (2024) 12:207–25. doi: 10.22034/cmde.2023.56140.2345
22. Bhan C, Karwarsa R, Malik S, Kumar S. Bifurcation, chaotic behavior, and soliton solutions to the KP-BBM equation through new Kudryashov and generalized Arnous methods. *AIMS Math*. (2024) 9:8749–67. doi: 10.3934/math.2024424
23. Arnous AH, Biswas A, Kara AH, Yildirim Y, Moraru L, Iticescu C, et al. Optical solitons and conservation laws for the concatenation model with spatio-temporal dispersion (internet traffic regulation). *J Eur Opt Soc Publ*. (2023) 19:35. doi: 10.1051/jeos/2023031
24. Arnous AH, Biswas A, Kara AH, Yildirim Y, Moraru L, Iticescu C, et al. Optical solitons and conservation laws for the concatenation model: power-law nonlinearity. *Ain Shams Eng J*. (2024) 15:102381. doi: 10.1016/j.asej.2023.102381
25. Závada P. Operator of Fractional Derivative in the Complex Plane. *Commun Math Phys*. (1998) 192:261–85. doi: 10.1007/s002200050299
26. Li C, Dao X, Guo P. Fractional derivatives in complex planes. *Nonlinear Anal: Theory Methods Appl*. (2009) 71:1857–69. doi: 10.1016/j.na.2009.01.021
27. Guariglia E. Riemann zeta fractional derivative—functional equation and link with primes. *Adv Differ Equat*. (2019) 2019:261. doi: 10.1186/s13662-019-202-5
28. Guariglia E, Silvestrov S. A functional equation for the Riemann zeta fractional derivative. In: *AIP Conference Proceedings*. New York: AIP Publishing (2017). p. 020063.
29. Guariglia E. Fractional calculus, zeta functions and Shannon entropy. *Open Mathem*. (2021) 19:87–100. doi: 10.1515/math-2021-0010
30. Guariglia E. Fractional calculus of the Lerch Zeta function. *Med J Mathem*. (2022) 19:109. doi: 10.1007/s00009-021-01971-7
31. Agarwal P, Nieto JJ. Some fractional integral formulas for the Mittag-Leffler type function with four parameters. *Open Mathem*. (2015) 13:537–46. doi: 10.1515/math-2015-0051
32. Rabie WB, Ahmed HM, Darwish A, Hussein HH. Construction of new solitons and other wave solutions for a concatenation model using modified extended tanh-function method. *Alexandria Eng J*. (2023) 74:4451–76. doi: 10.1016/j.aej.2023.05.046
33. Nasreen N, Lu D, Zhang Z, Akgül A, Younas U, Nasreen S, et al. Propagation of optical pulses in fiber optics modelled by coupled space-time fractional dynamical system. *Alexandria Eng J*. (2023) 73:173–87. doi: 10.1016/j.aej.2023.04.046
34. Russell JS. *Report on Waves: Made to the Meetings of the British Association in 1842-43*. United Kingdom: British Association for the Advancement of Science. (1842).
35. Korteweg DJ, de Vries G. On the change of form of long waves advancing in a rectangular canal, and on a new type of long stationary waves. *Philosoph Magazine, Series 5*. (1895) 39:422–43. doi: 10.1080/14786449508620739
36. Zabusky NJ, Kruskal MD. Interaction of "Solitons" in a Collisionless Plasma and the Recurrence of Initial States. *Phys Rev Lett*. (1965) 15:240–3. doi: 10.1103/PhysRevLett.15.240
37. Gardner CS, Greene JM, Kruskal MD, Miura RM. Method for solving the Korteweg–de Vries equation. *Phys Rev Lett*. (1967) 19:1095–7. doi: 10.1103/PhysRevLett.19.1095
38. Wadati M. Introduction to Solitons. *Pramana - J Phys*. (2001) 57:841–7. doi: 10.1007/s12043-001-0002-3
39. Khalil R, Horani MA, Yousef A, Sababheh M, A. new definition of fractional derivative. *J Comput Appl Math*. (2014) 264:65–70. doi: 10.1016/j.cam.2014.01.002
40. Agarwal P, Choi J, Paris RB, A. novel numerical dynamics of fractional derivatives involving singular and nonsingular kernels: designing a stochastic cholera epidemic model. *AIMS Mathematics*. (2021) 6:4544–63. doi: 10.1016/B978-0-12-397023-7.00011-5
41. Agrawal GP. *Nonlinear Fiber Optics*. 5th ed. Cambridge, MA: Academic Press. (2013). doi: 10.1016/B978-0-12-397023-7.00011-5
42. Sasa N, Satsuma J. New-type of soliton solutions for a higher-order nonlinear Schrödinger equation. *J Phys Soc Japan*. (1991) 60:409–17. doi: 10.1143/JPSJ.60.409
43. Mahmud F, Samsuzzoha M, Akbar MA. The generalized Kudryashov method to obtain exact traveling wave solutions of the PHI-four equation and the Fisher equation. *Results Phys*. (2017) 7:4296–302. doi: 10.1016/j.rinp.2017.10.049
44. Ozisik M, Secer A, Bayram M, Aydin H, A. new definition of Kudryashov's integrability approaches applicable to optoelectronics. *Optik (Stuttg)*. (2022) 265:169499. doi: 10.1016/j.ijleo.2022.169499
45. Herman R. Solitary waves. *Am Sci*. (1992) 80:350–61.
46. Li YY, Jia HX, Zuo DW. Multi-soliton solutions and interaction for a (2+1)-dimensional nonlinear Schrödinger equation. *Optik*. (2021) 241:167019. doi: 10.1016/j.ijleo.2021.167019